Journal of Molecular Liquids 337 (2021) 116541

Contents lists available at ScienceDirect

Journal of Molecular Liquids

journal homepage: www.elsevier.com/locate/molliq

Chemical, electrochemical, theoretical (DFT & MEP), thermodynamics and surface morphology studies of carbon steel during gas and oil production using three novel di-cationic amphiphilies as corrosion inhibitors in acidic medium

M.A. Hegazy [a,*], M.M. Hegazy [b], M.K. Awad [c], M. Shawky [d]

[a] Egyptian Petroleum Research Institute (EPRI) Nasr City, Cairo, Egypt
[b] Chemistry Dept., Faculty of Science, Helwan University, Cairo, Egypt
[c] Theoretical Applied Chemistry Unit, Chemistry Department, Faculty of Science, Tanta University, Tanta, Egypt
[d] General Petroleum Company (GPC), Cairo, Egypt

ARTICLE INFO

Article history:
Received 21 February 2021
Revised 3 May 2021
Accepted 18 May 2021
Available online 21 May 2021

Keywords:
Di-cationic surfactant
EIS
Tafel
SEM
AFM
Molecular modeling
DFT

ABSTRACT

Three di-cationic amphiphilies were synthesized and characterized by FTIR, (^{1}H & ^{13}C) NMR spectroscopies. These compounds are tested as corrosion inhibitors for CS in 1 M HCl by weight loss (WL), EIS, potentiodynamic polarization (PP) techniques, and surface morphology (SEM & AFM). Surface tension results exhibited that these surfactants are a good surface attitude in their aqueous media. The gained results exhibited that the di-cationic surface-active agents are stellar deterioration inhibitors for CS in 1 M HCl. A discouragement efficacy augmented with increment of the inhibitor concentration. Adsorption of CSI, CSII & CSIII on CS in 1 M HCl was established to comply with Langmuir's adsorption isotherm. SEM & AFM photos exhibit a good CS surface in presence of CSI, CSII & CSIII in opposite of the absence of them. The inhibition mechanism is suggested on the thermodynamic factors. The inhibitive impact of the explored surfactants against the corrosion of the CS surface was implied by DFT/6-31G (d,p) computations.

1. Introduction

In the oil field, there is an acidizing process involves the injection of chemicals to improve the flow of reservoir fluids, usually HCl (strong acid) is used to dissolve rock formations [1]. During the acetification operation, it is needful to clean off the isolated oxide but the metal is more susceptible to corrosion after the pickling process so it is very important to use corrosion inhibitors [2,3]. CS has been commonly utilized in oil and gas production like recovery tubes, flux pipelines, and shipping lines [4]. Preventing the corrosion of CS is very important in numerous manufactures. Many studies are offered effective methods for the suppression of corrosion. The cationic surfactants reduce a metal dissolution rate where the action of the cationic surfactants in an acidic medium is adsorption onto a steel surface. The technique of corrosion discouragement depends on an adsorption of a surfactant on metallic surfaces. Then substitution water by inhibitor to form a layer which keeps metal verse corrosion [5]. The adsorption process relies on the nature of a metal surface, type of corrosive environment, and chemical composition of the CSI, CSII & CSIII. Adsorption places because of the interrelation between the free & π electron of inhibitor and orbitals of metallic surface atoms. This interrelation exhibits a good adsorption of an inhibitor onto a metallic face leads to a composition of a protective layer. The high suppression performance of the CSI, CSII & CSIII comes from the switching of distinct heteroatoms (ex. N, O, Cl and Br) and a subsistence of π-electrons in their structures. These compounds form a very thin layer and adsorbed layer that lead to a reduction in the corrosion rate [6]. The election of an inhibitor is controlled by its capability to damp corrosion on a metal face and its environmental impacts. They are organic materials that contain N, S, O, and P to reduce a corrosion attack on CS [7]. The cationic surfactants lowering the corrosion rate by adsorbing on a metal surface, and prohibit the active sites insecure with a corrosive media on the metal surface [8,9].

Exploratory methods are valuable in clarifying the mechanism of inhibition yet they are regularly costly and tedious. Continuous equipment and programming propels have opened the entryway for ground-breaking utilization of computational chemistry in

* Corresponding author.
E-mail address: mohamed_hgazy@yahoo.com (M.A. Hegazy).

https://doi.org/10.1016/j.molliq.2021.116541
0167-7322/

corrosion hindrance research. In this way, a few quantum chemical strategies and modeling displaying methods have been acted as correspond the inhibition efficacy of the properties of substances [10-13]. The utilization of hypothetical quantum parameters exhibit two principal focal points: firstly, the materials with their different sections and substituents can be straightforwardly described based on their molecular constructions just; and secondly, the suggested reaction mechanization of association can be straightforwardly represented regarding the synthetic reactivity of compounds [14]. A few examinations have demonstrated that the hindrance of corrosion is essentially portrayed by an arrangement of contributor donor–acceptor face buildings betwixt free or $\pi-$ electrons of a surfactant, generally comprising N, S, or O particles, and goofy d-orbital of a metal [15-17]. Di-cationic surfactants which are significant mixtures in numerous scopes have been accounted for before as consumption inhibitors for a metal [18].

The target of research is to explore the influence of three di-cationic surfactants namely: (*E*)-*N*-(2-(2-((2-(((furan-2-ylmethylene)amino)ethyl)dimethylammonio)acetoxy)ethyl)-*N*,*N*-dimethyl dodecan-1-aminium bromide chloride (**CSI**), *N*-(2-(2-(dimethyl(2-(((1*E*,2*E*)-3-phenylallylidene) amino)ethyl)ammonio)acetoxy)ethyl)-*N*,*N*-dimethyldodecan-1-aminium bromide chloride (**CSII**), (*E*)-*N*-(2-(2-((2-((4-methoxybenzylidene)amino)ethyl)dimethylammonio)acetoxy)ethyl)-*N*,*N*-dimethyldodecan-1-aminium bromide chloride (**CSIII**) on CS in 1 M HCl medium through chemical (WL) and electrochemical (PP & EIS) procedures. We study surface parameters to determine the optimum dose of inhibitors. We study the inhibition behavior of di-cationic amphiphilies on the CS face through thermodynamic parameters to understanding the corrosion suppression technique and interactivity betwixt the inhibitor molecules and CS surface. Surface inspection (SEM & AFM) is used for the examination of the steel surface with and without CSI, CSII & CSIII. The relationship between the structural parameters and corrosion inhibition of those compounds has not been studied yet. Therefore the task of this paper is to correlate the quantum chemical parameters and the observed inhibition efficiency of the investigated surfactant inhibitors. The inhibitive impact of the explored surfactants against the corrosion of the surface of CS was implied by DFT/6-31G(d,p) computations. The determined quantum parameters associated with the restraint effectiveness are lowest unoccupied molecular orbital(LUMO), highest occupied molecular orbital (HOMO), separation gap (ΔE), dipole moment (*DM*), softness (σ), total negative charge (*TNC*), molecular volume (*MV*), chemical potential (μ), and electronegativet (χ). A decent relationship was found between the exploratory and hypothetical examinations. The relationship betwixt the parameters and corrosion restraint of those compounds has not been performed at this point. The undertaking of this search is to relate the quantum variables and the noticed corrosion hindrance proficiency of the examined surfactants.

2. Experimental methods and materials

2.1. Synthesis

Three di-cationic surfactants (CSI, CSII & CSIII) applied in a search were produced through four steps:

The first step:

Three Schiff bases were synthesized by reaction (8.815 g, 0.1 mol) N^1,N^1-dimethylethane-1,2-diamine with (9.609 g, 0.1 mol) Furan-2-carbaldehyde, (13.216 g, 0.1 mol) Cinnamaldehyde, and (13.615 g, 0.1 mol) 4-methoxybenzaldehyde in 100 ml absolute ethanol at 70 °C for 6 h. Then evaporate the amount of ethanol. The products were recrystallized by hot ethanol. The products purified by diethyl ether [19] to produce (*E*)-2-((furan-2-ylmethylene)amino)-*N*,*N*-dimethylethan-1-amine (viscous and black color), *N*,*N*-dimethyl-2-(((1*E*,2*E*)-3-phenylallylidene)amino) ethan-1-amine (semi-liquid and black red color), and (*E*)-2-((4-methoxybenzylidene)amino)-*N*,*N*-dimethylethan-1-amine (semi-liquid and black red color) respectively, as in Scheme 1.

The second step:

Reaction (8.914 g, 0.1 mol) 2-(Dimethylamino)ethan-1-ol and (24.923 g, 0.1 mol) 1-bromododecane in 100 ml absolute ethanol at 70 °C for two days. The products recrystallized by hot ethanol and purified by diethyl ether. The product N-(2-hydroxyethyl)-N, N-dimethyldodecan-1-aminium bromide (white powder) is shown in Scheme 2.

The third step:

Reaction (33.837 g, 0.1 mol) *N*-(2-hydroxyethyl)-*N*,*N*-dimethyldodecan-1-aminium bromide and (9.449 g, 0.1 mol) Chloroacetic acid in 100 ml xylene till percent of water which calculated is trapped. And evaporate xylene from a mixture then let the mixture cool down, and finally *N*-(2-(2-chloroacetoxy)ethyl)-*N*,*N*-dimethyldodecan-1-aminium bromide (honey color- viscous liquid) as in Scheme 2.

The fourth step:

Reaction of (41.485 g, 0.1 mol) *N*-(2-(2-chloroacetoxy)ethyl)-*N*, *N*-dimethyldodecan-1-aminium bromide and (16.622 g, 0.1 mol) (*E*)-2-((furan-2-ylmethylene)amino)-*N*,*N*-dimethylethan-1-amine, (20.230 g, 0.1 mol) *N*,*N*-dimethyl-2-(((1*E*,2*E*)-3-phenylallylidene)amino)ethan-1-amine, and (20.629 g, 0.1 mol) (*E*)-2-((4-methoxybenzylidene)amino)-*N*,*N*-dimethylethan-1-amine in 100 ml absolute ethanol at 70 °C for two days.

Then evaporate ethanol from the mixture and let the mixture to cool-down. To produce (*E*)-*N*-(2-(2-((2-((furan-2-ylmethylene)amino)ethyl)dimethylammonio)acetoxy)ethyl)-*N*,*N*-dimethyldodecan-1-aminium bromide chloride (**CSI**) (black-brown viscous), *N*-(2-(2-(dimethyl(2-(((1*E*,2*E*)-3-phenylallylidene)amino) ethyl)ammonio)acetoxy)ethyl)-*N*,*N*-dimethyldodecan-1-aminium bromide chloride (**CSII**) (black-brown semi-liquid), and (*E*)-*N*-(2-(2-((2-((4-methoxybenzylidene)amino)ethyl)dimethylammonio) acetoxy)ethyl)-*N*,*N*-dimethyldodecan-1-aminium bromide chloride (**CSIII**) (black-brown semi-liquid) as in Scheme 3.

2.2. Surface tension

Surface properties is evaluated via utilizing Kruss K6 tensiometer for CSI, CSII & CSIII with a concentration of (5×10^{-5}–1×10^{-3}M) at 25 °C.

2.3. Weight loss technique

Analytical balance, (KERN Pattern: ABJ 320-4NM), was used for weight loss evaluation. The CS coupons of $6 \times 3 \times 0.4$ CM were rubbed off with emery sheets (degree 320–400–600–800–1000–1200–2500) then wash out by DW, acetone, and lastly dry with air. After carefully weighing, coupons are placed in 100 ml volume 1 M HCl medium in occurrence & absenteeism of various concentrations of surfactants at varied temperatures. Temperatures of weight loss evaluations were stripped by water bath supplied by thermostat 0.5 °C. The CS coupons were taken out after 24 h then immersed in inhibited 15% HCl solution to remove corrosion products then immersed in saturated sodium bicarbonate for one minute to equalize the acid, then wash with distilled water to cut off the neutralizer, then wash the coupons in acetone, and dry the coupons with dry air. Finally, weight and record the results in mg. The chemical structure of AISI 1018 mild/low CS specimen has a following percentage of elements: C (0.14–0.20), Mn (0.60–0.90), P $\leq$ 0.040, S 0.050, Fe (98.81–99.26% as remainder).

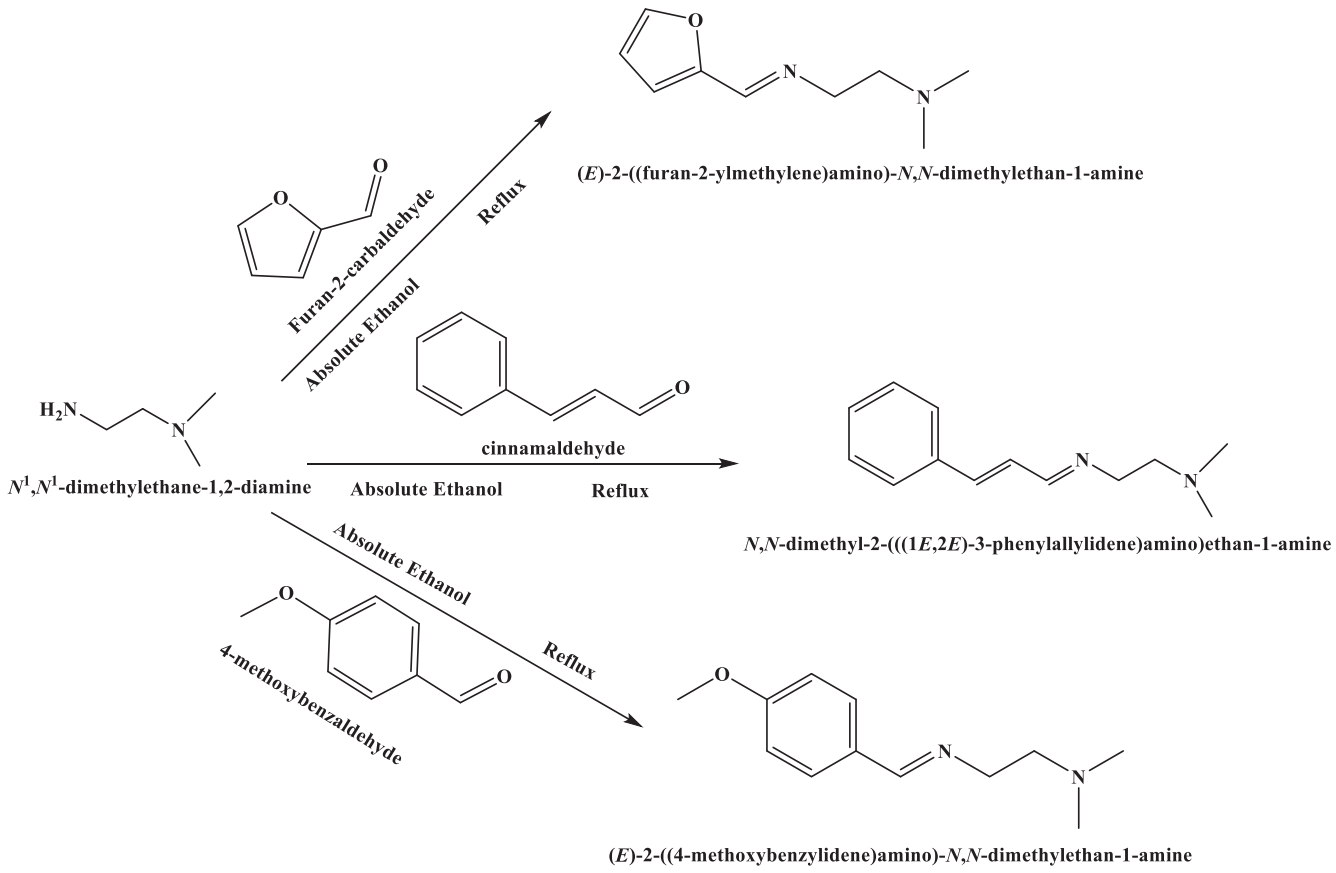

Scheme 1.

2.4. Electrochemical measurements

The electrochemical studies are achieved in a suitable three-electrode cell with a platinum counter electrode (CE) and a saturated calomel electrode (SCE) as a reference electrode. The working electrode (WE) is a rod of CS included in PVC holder utilizing Teflon. Therefore, a regular face was the lone uncovered face in the electrode. Uncovered area is 0.7 cm^2 for working. Such region is rubbed off with an emery sheet (degree 320–400–600–800–1000–1200–2500) on the test surface, and then immersed in DW, then acetone, and lastly drying with dry atmosphere.

Prior evaluation, the electrode is sunken in a test solution at (OCP) for half hour until a steady state was attained. All electrochemical evaluations were accomplished by utilizing a Volta Lab 40 (PGZ 301 & Volta master 4) - (Radiometer Analytical - FRANCE) at 25 °C. The potentiodynamic polarization measures were acquired by alteration the electrode potential from −800 to −200 mV versus SCE at 25 °C. EIS measurements were applied in the frequency range of 100 kHz – 30 mHz at a little alternating voltage perturbation (10 mV) at 20 °C.

2.5. SEM and AFM image

SEM (Inspect S, Manufacturer FEI Company, Netherlands) and Atomic Force Microscope (AFM, MFP, Asylum Research) that give 3-D photo are used as a powerful tool in the morphological examinations for CS surface immersed for one day in 1 M HCl in an absenteeism and an existence of 1×10^{-3}M of CSI, CSII & CSIII at 25 °C.

2.6. Theory and computational details:

The molecular structures of the investigated di- cationic surfactants were optimized with the DFT/6-31G (d,p) method. A vibrational investigation of the structures is executed by Gaussian 09 program package [20] to decide if they match to a maximal or a minimal on a potential energy bend and found imaginative was determined, showing minimum energy structure. The matters were worked with the GaussView 5.0 executed in Gaussian 09. Molecular orbitals (HOMOandLUMO) could be utilized to anticipate the center of adsorption of the inhibitors. For ordinary exchange of electrons, adsorption ought to happen at the piece of a particle where the softness(σ), which is a property that has the most elevated worth.

3. Results and discussion

3.1. Chemical structure validation

The chemical structure was established by FTIR, ^{1}HNMR & ^{13}CNMR spectroscopies.

3.1.1. Confirmation of Schiff bases structure

FTIR of **Schiff base (I)** exhibited the following absorption sects at 1011.93 cm^{-1} (C—N stretch), 1378.4 cm^{-1} (C—H rock), 1462.47 cm^{-1} (C—H bend), 1664.85 cm^{-1} (C═N stretch), 2859.5 cm^{-1} (C—H stretch), 2941.4 cm^{-1} (═C—H stretch) as displayed in (**Supplementary materials,** Fig. 1).

FTIR of **Schiff base (II)** exhibited the following absorption sects at 1035.29 cm^{-1} (C—N stretch), 1381.34 cm^{-1} (C—H rock),

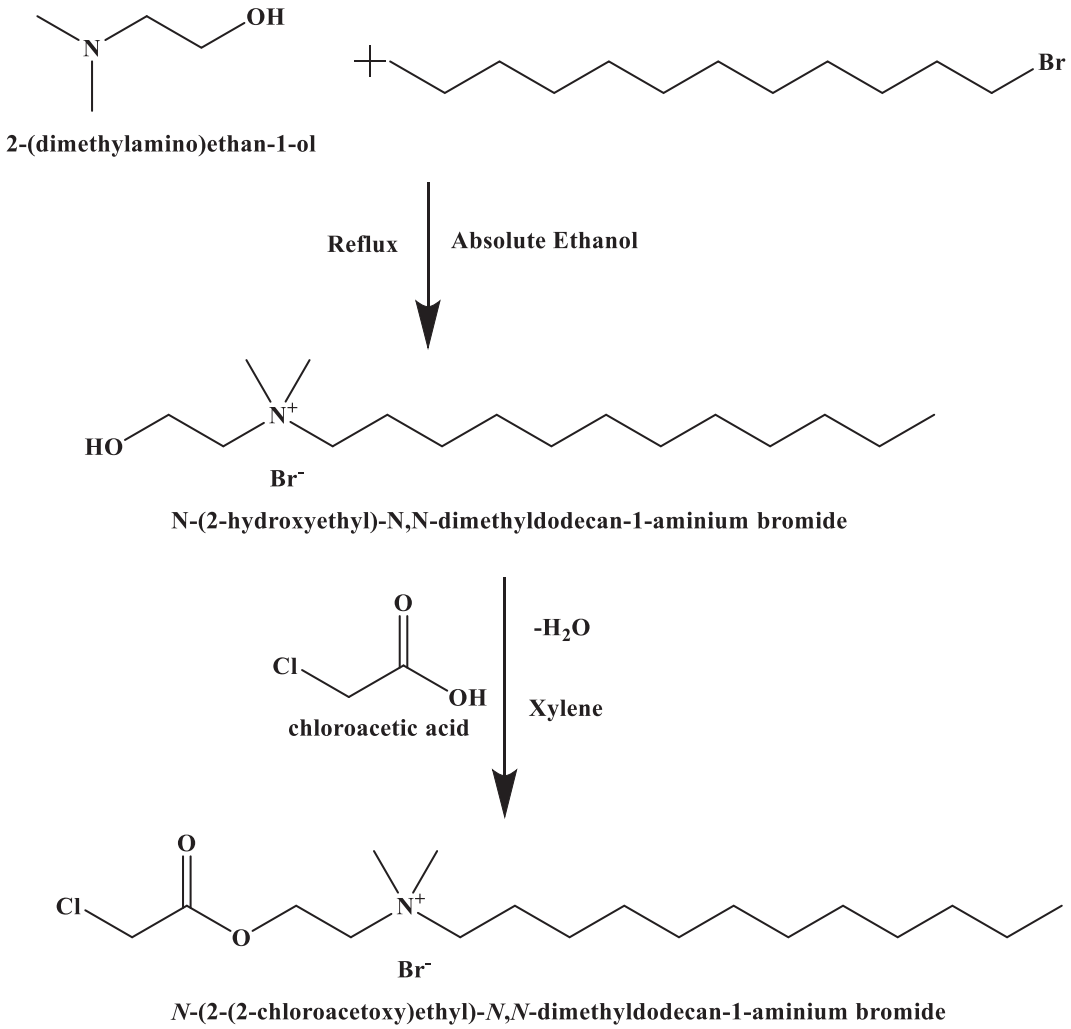

Scheme 2.

1453.62 cm^{-1} (C—H bending), 1634.93 cm^{-1} (C=N stretch), 1672.17 cm^{-1} (C=C stretch), 2859.34 cm^{-1}(C—H stretch), 2943.52 cm^{-1}(=C—H stretch) as shown in (**Supplementary materials,** Fig. 2).

FTIR of **Schiff base (III)** exhibited the following absorption sects at 1032.24 cm^{-1} (C—N stretch), 1379.59 cm^{-1} (C—H rock), 1461.77 cm^{-1} (C—H bend), 1645.26 cm^{-1} (C=N stretch), 2833.4 cm^{-1} (C—H stretch), 2941.45 cm^{-1} (=C-H stretch) as shown in (**Supplementary materials,** Fig. 3).

3.1.2. Validation of monomeric surfactant (product of step 2)

FTIR of **step (2)** product exhibited the following absorption sects at 1084.87 cm^{-1} (C—N stretch), 1378.34 cm^{-1} (C—H rock), 1468.37 cm^{-1}(C—H bend), 2853.54 cm^{-1}(C—H stretch), 3398.3 cm^{-1} (O—H stretch) as shown in (**Supplementary materials,** Fig. 4).

^{1}HNMR of **step (2)** product exhibited different beaks at δ = 0.85 ppm (t, 3H, $NCH_2(CH_2)_nCH_2C\underline{H}_3$); δ = 1.27 ppm (m, 6H, $NCH_2(CH_2)_nC\underline{H}_2CH_3$); δ = 1.25 ppm (m, 5H, $NCH_2(C\underline{H}_2)_nCH_2CH_3$); δ = 1.65 ppm (s, 3H, $NC\underline{H}_2(CH_2)_nCH_2CH_3$); δ = 3.29 ppm (s,1H, $NC\underline{H}3$); δ = 3.12 ppm (t, 3H, $HOCH_2C\underline{H}_2N$), δ = 3.38 ppm (m, 4H, $HOC\underline{H}_2CH_2N$), δ = 5.26 ppm (t, 3H, $\underline{H}OCH_2CH_2N$) as shown in Fig. 1.

3.1.3. Validation of the product of step 3

FTIR of **step (3)** product exhibited the following absorption sects at 1073.64 cm^{-1}(C—N stretch), 1400.27 cm^{-1} (C—H rock), 1464.7 cm^{-1} (C—H bend), 1197.84 cm^{-1} (C—O stretch), 1747.33 cm^{-1} (C=O stretch), 2853.47 cm^{-1} (C—H stretch). The FTIR assured the predicted function groups in the step (3) product as shown in (**Supplementary materials,** Fig. 5).

^{1}HNMR of **step (3)** product exhibited different sects at δ = 0.85 ppm (t, 3H, $NCH_2(CH_2)_nCH_2C\underline{H}_3$); δ = 1.22 ppm (m, 6H, $NCH_2(CH_2)_nC\underline{H}_2CH_3$); δ = 1.22 ppm (m, 5H, $NCH_2(C\underline{H}_2)_nCH_2CH_3$); δ = 1.52 ppm ($NC\underline{H}_2(CH_2)_n\ CH_2CH_3$); δ = 2.73 ppm (s, 1H, $NC\underline{H}_3$); δ = 2.49 ppm (t, 3H, $ClCH_2COOCH_2C\underline{H}_2N$), δ = 3.04 ppm (t, 3H, $ClCH_2COOC\underline{H}_2CH_2N$), δ = 3.46 ppm ((s, 1H, $ClC\underline{H}_2COOCH_2CH_2N$) as shown in (**Supplementary materials,** Fig. 6).

^{13}CNMR of **step (3)** product exhibited various sects at δ = 13.97 ppm ($NCH_2(CH_2)_nCH_2CH_2\underline{C}H_3$); δ = 22.12 ppm ($NCH_2(-CH_2)_nCH_2\underline{C}H_2CH_3$); δ = 31.33 ppm ($NCH_2(CH_2)_n\underline{C}H_2CH_2CH_3$); δ = 28.99 ppm ($NCH_2(\underline{C}H_2)_nCH_2CH_2CH_3$); δ = 68.54 ppm ($N\underline{C}H_2(CH_2)_nCH_2CH_2CH_3$); δ = 54.22 ppm ($N\underline{C}H_3$); δ = 68.54 ppm ($ClCH_2COOCH_2\underline{C}H_2N$), δ = 59.58 ppm ($ClCH_2COO\underline{C}H_2CH_2N$), δ = 168.56 ppm ($ClCH_2\underline{C}OOCH_2CH_2N$), δ = 48.24 ppm ($Cl\underline{C}H_2-COOCH_2CH_2N$) as shown in Fig. 2.

3.1.4. Validation of CSI, CSII & CSIII

FTIR of (**CSI**) exhibited the following absorption sects at 1077.67 cm^{-1} (C—N stretch), 1378.01 cm^{-1} (C—H rock), 1465.75 cm^{-1} (C—H bend), 1149.24 cm^{-1} (C—O stretch), 1660.35 cm^{-1} (C=O stretch), 2854.13 cm^{-1} (C—H stretch),

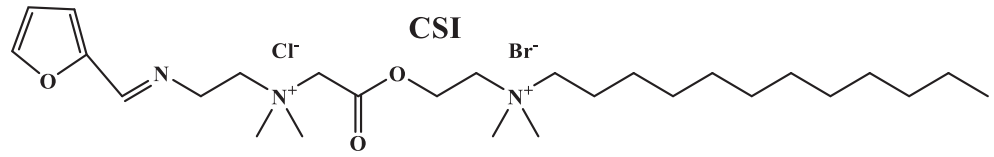

(*E*)-*N*-(2-(2-((2-((furan-2-ylmethylene)amino)ethyl)dimethylammonio)acetoxy)ethyl)-*N*,*N*-dimethyldodecan-1-aminium bromide chloride

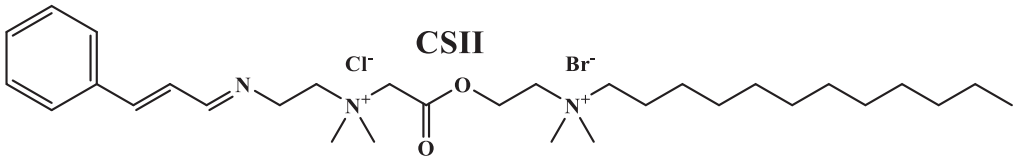

***N*-(2-(2-(dimethyl(2-(((1*E*,2*E*)-3-phenylallylidene)amino)ethyl)ammonio)acetoxy)ethyl)-*N*,*N*-dimethyldodecan-1-aminium bromide chloride**

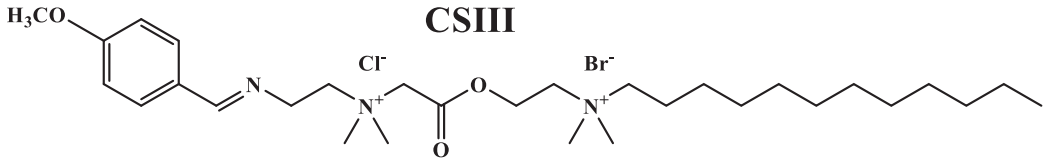

(*E*)-*N*-(2-(2-((2-((4-methoxybenzylidene)amino)ethyl)dimethylammonio)acetoxy)ethyl)-*N*,*N*-dimethyldodecan-1-aminium bromide chloride

Scheme 3.

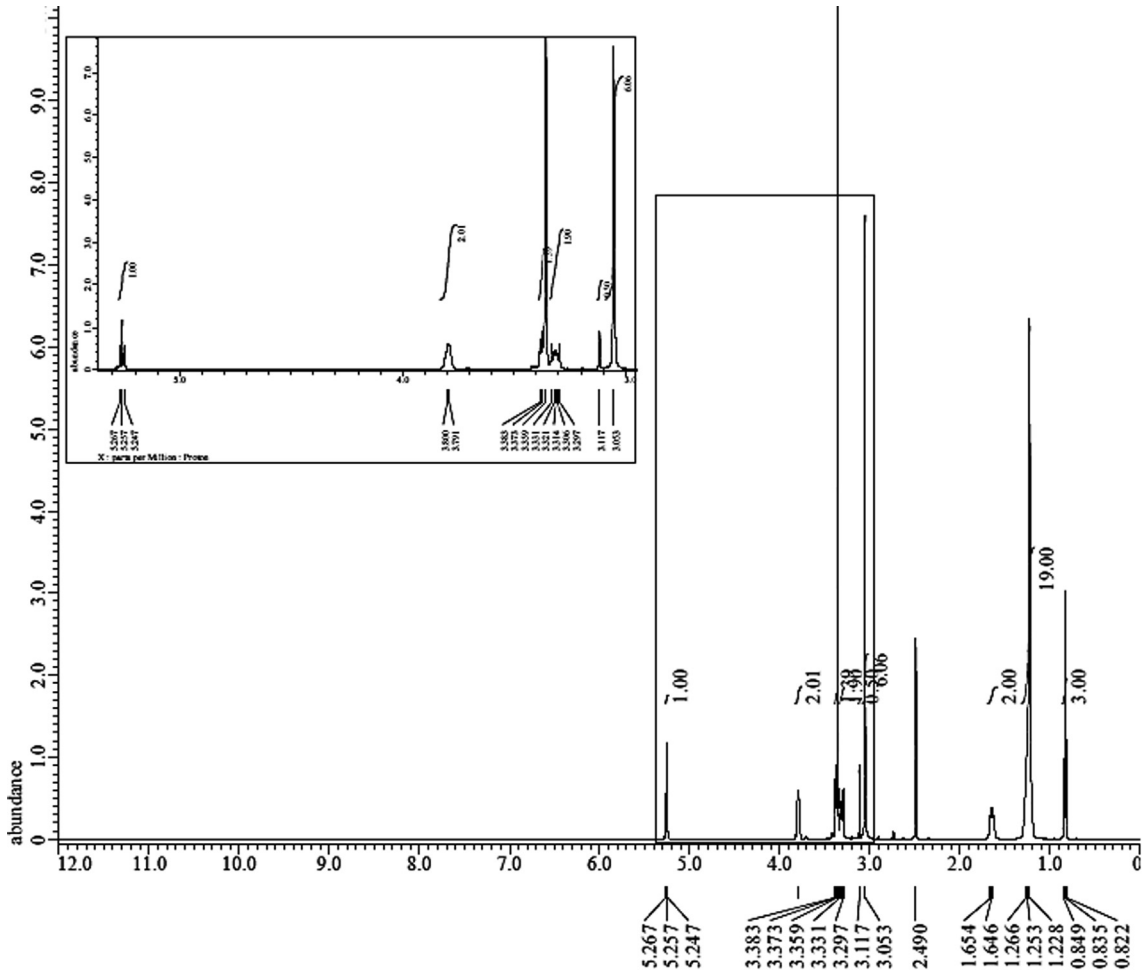

Fig. 1. [1]HNMR of step (2) product.

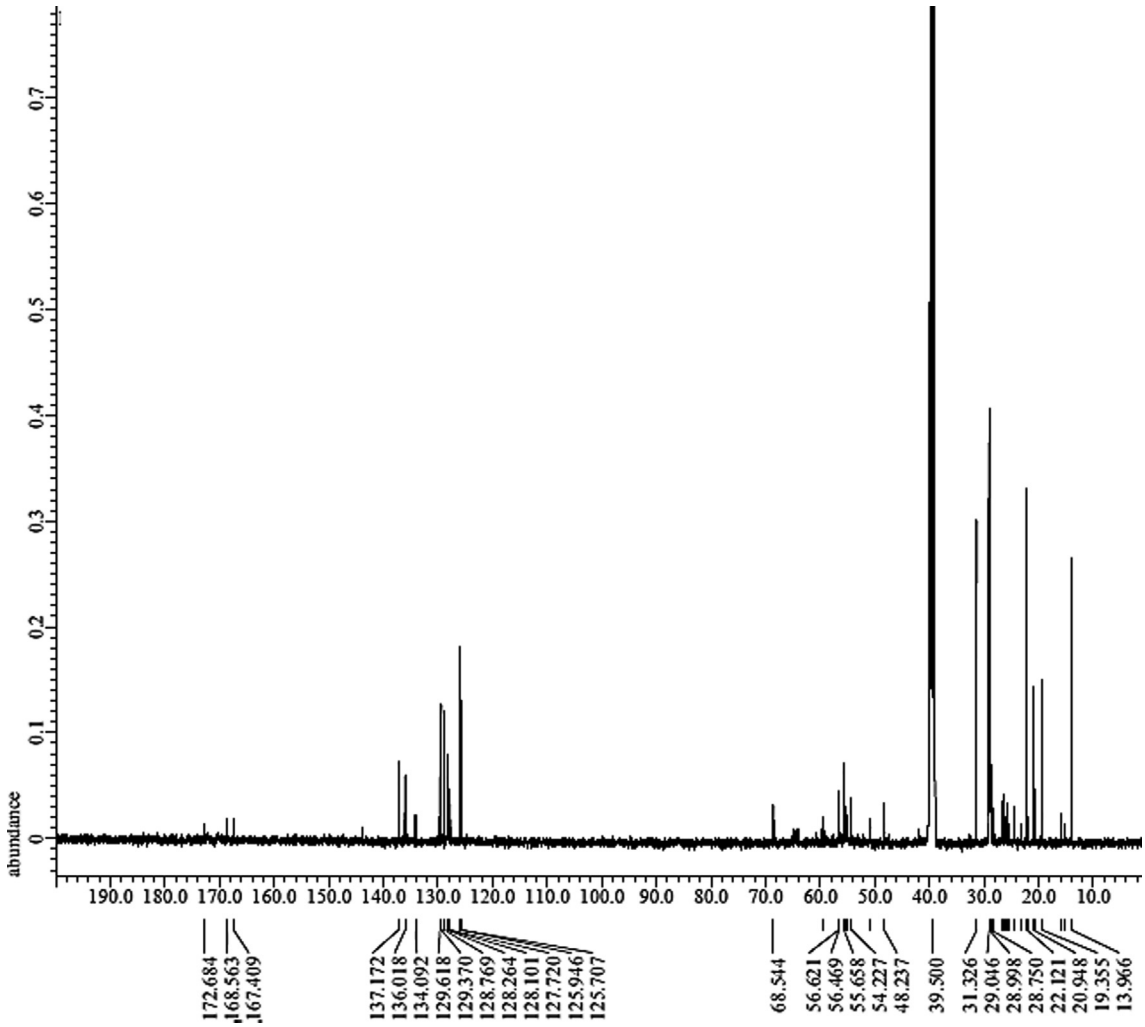

Fig. 2. ^{13}CNMR of step (3) product.

2925.14 cm^{-1} (=C—H stretch) as shown in (**Supplementary materials,** Fig. 7).

FTIR of (**CSII**) exhibited the following absorption sects at 1071.90 cm^{-1} (C—N stretch), 1378.25 cm^{-1} (C—H rock), 1463.66 cm^{-1} (C—H bend), 1648.43 cm^{-1} (C=C stretch), 1152.31 cm^{-1} (C—O stretch), 1744.7 cm^{-1}(C=O stretch), 2853.76 cm^{-1}(C—H stretch), 2924.95 cm^{-1}(=C—H stretch) as shown in (**Supplementary materials,** Fig. 8).

FTIR of (**CSIII**) exhibited the following absorption sects at 1034.61 cm^{-1} (C—N stretch), 1374.69 cm^{-1} (C—H rock), 1512.41 cm^{-1} (C—H bend), 1168.95 cm^{-1} (C—O stretch), 1744.55 cm^{-1} (C=O stretch), 2853.54 cm^{-1} (C—H stretch), 2925.45 cm^{-1} (=C—H stretch) as shown in (**Supplementary materials,** Fig. 9).

^{1}HNMR of (**CSI**) exhibited different sects at δ = 0.88 ppm (t, 3H, $NCH_2(CH_2)_nCH_2C\underline{\mathbf{H}}_3$), δ = 1.3 ppm (m, 6H, $NCH_2(CH_2)_nC\underline{\mathbf{H}}_2CH_3$), δ = 1.7 ppm (m, 5H, $NCH_2(C\underline{\mathbf{H}}_2)_nCH_2CH_3$), δ = 3.2 ppm (t, 3H, $NC\underline{\mathbf{H}}_2(-CH_2)_nCH_2CH_3$), δ = 3.3 ppm (s, 1H, $NC\underline{\mathbf{H}}_3$), δ = 3.5 ppm (t, 3H, $NCH_2-COOCH_2C\underline{\mathbf{H}}_2N$), δ = 4.2 ppm (t, 3H, $NCH_2COOC\underline{\mathbf{H}}_2CH_2N$), δ = 3.9 ppm (s, 1H, $NC\underline{\mathbf{H}}_2COOCH_2CH_2N$), δ = 3.2 ppm (t, 3H, Ar-CH=N $CH_2-COOCH_2C\underline{\mathbf{H}}_2N$), δ = 1.9 ppm (t, 3H, Ar-CH=$NCH_2COOC\underline{\mathbf{H}}_2CH_2N$), δ = 7.9 ppm (s, 1H, Ar-C$\underline{\mathbf{H}}$=N $CH_2COOCH_2CH_2N$) as shown in Fig. 3.

^{1}HNMR of (**CSII**) exhibited different sects at δ = 0.86 ppm (t, 3H, $NCH_2(CH_2)_nCH_2C\underline{\mathbf{H}}_3$), δ = 1.23 ppm (m, 6H, $NCH_2(CH_2)_nC\underline{\mathbf{H}}_2CH_3$), δ = 1.54 ppm (m, 5H, $NCH_2(C\underline{\mathbf{H}}_2)_nCH_2CH_3$), δ = 3.01 ppm (t, 3H, $NC\underline{\mathbf{H}}_2(CH_2)_nCH_2CH_3$), δ = 3.03 ppm (s, 1H, $NC\underline{\mathbf{H}}_3$), δ = 3.09 ppm (t, 3H, $NCH_2COOCH_2C\underline{\mathbf{H}}_2N$), δ = 3.97 ppm (t, 3H, $NCH_2COOC\underline{\mathbf{H}}_2CH_2N$), δ = 3.47 ppm (s, 1H, $NC\underline{\mathbf{H}}_2COOCH_2CH_2N$), δ = 3.03 ppm (t, 3H, Ar-CH=CHCH=$NCH_2C\underline{\mathbf{H}}_2N$), δ = 1.8 ppm (t, 3H, Ar-CH=CHCH=$NC\underline{\mathbf{H}}_2CH_2N$), δ = 7.89 ppm (d, 2H, Ar-CH=CH$C\underline{\mathbf{H}}$=NCH_2CH_2N), δ = 7.14 ppm (t, 3H, Ar-CH=C$\underline{\mathbf{H}}$CH=NCH_2CH_2N), δ = 7.29 ppm (d, 2H, Ar-C$\underline{\mathbf{H}}$=CHCH=NCH_2CH_2N) as shown in Fig. 4.

^{1}HNMR of (**CSIII**) exhibited different sects at δ = 0.85 ppm (t, 3H, $NCH_2(CH_2)_nCH_2C\underline{\mathbf{H}}_3$), δ = 1.22 ppm (m, 6H, $NCH_2(CH_2)_nC\underline{\mathbf{H}}_2CH_3$), δ = 1.58 ppm (m, 5H, $NCH_2(C\underline{\mathbf{H}}_2)_nCH_2CH_3$), δ = 2.95 ppm (t, 3H, $NC\underline{\mathbf{H}}_2(CH_2)_nCH_2CH_3$), δ = 3.1 ppm (s, 1H, $NC\underline{\mathbf{H}}_3$), δ = 3.45 ppm (t, 3H, $NCH_2COOCH_2C\underline{\mathbf{H}}_2N$), δ = 3.85 ppm (t, 3H, $NCH_2COOC\underline{\mathbf{H}}_2CH_2N$), δ = 3.71 ppm (s, 1H, $NC\underline{\mathbf{H}}_2COOCH_2CH_2N$), δ = 2.95 ppm (t, 3H, Ar-CH=$NCH_2C\underline{\mathbf{H}}_2N$), δ = 3.73 ppm (t, 3H, Ar-CH=$NC\underline{\mathbf{H}}_2CH_2N$), δ = 8.3 ppm (s, 1H, Ar-C$\underline{\mathbf{H}}$=NCH_2CH_2N), δ = 3.78 ppm (s, 1H, $OC\underline{\mathbf{H}}_3$) as shown in Fig. 5.

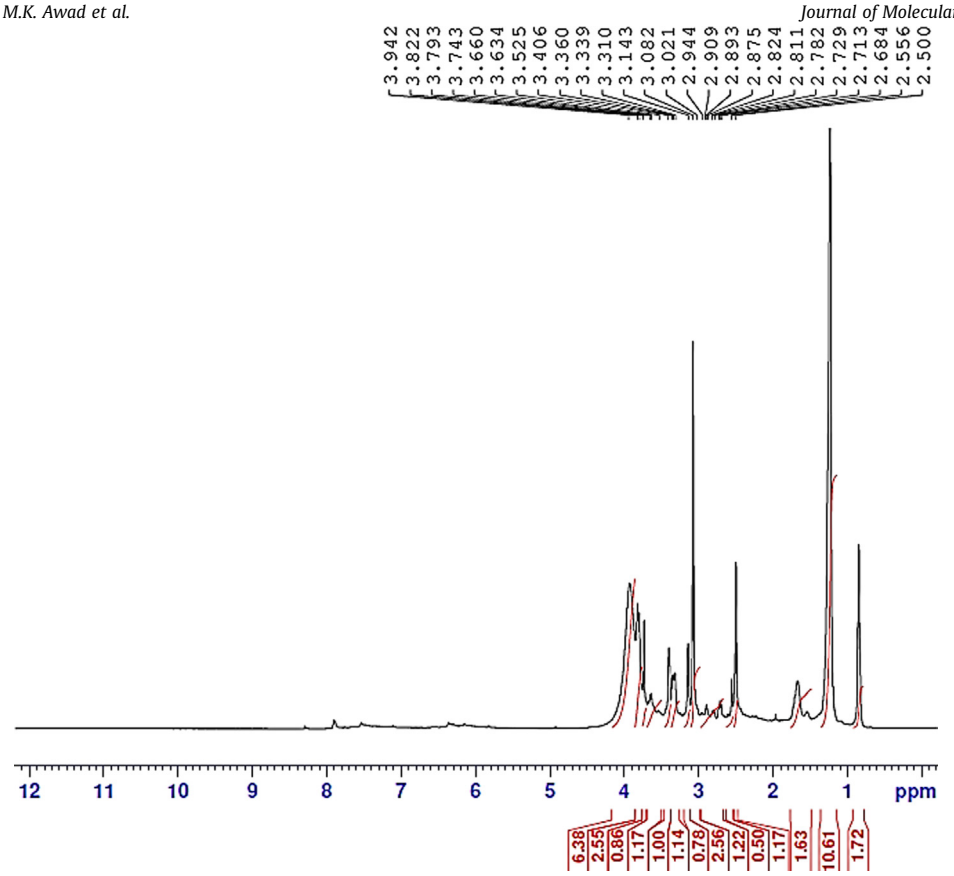

Fig. 3. [1]HNMR of CSI.

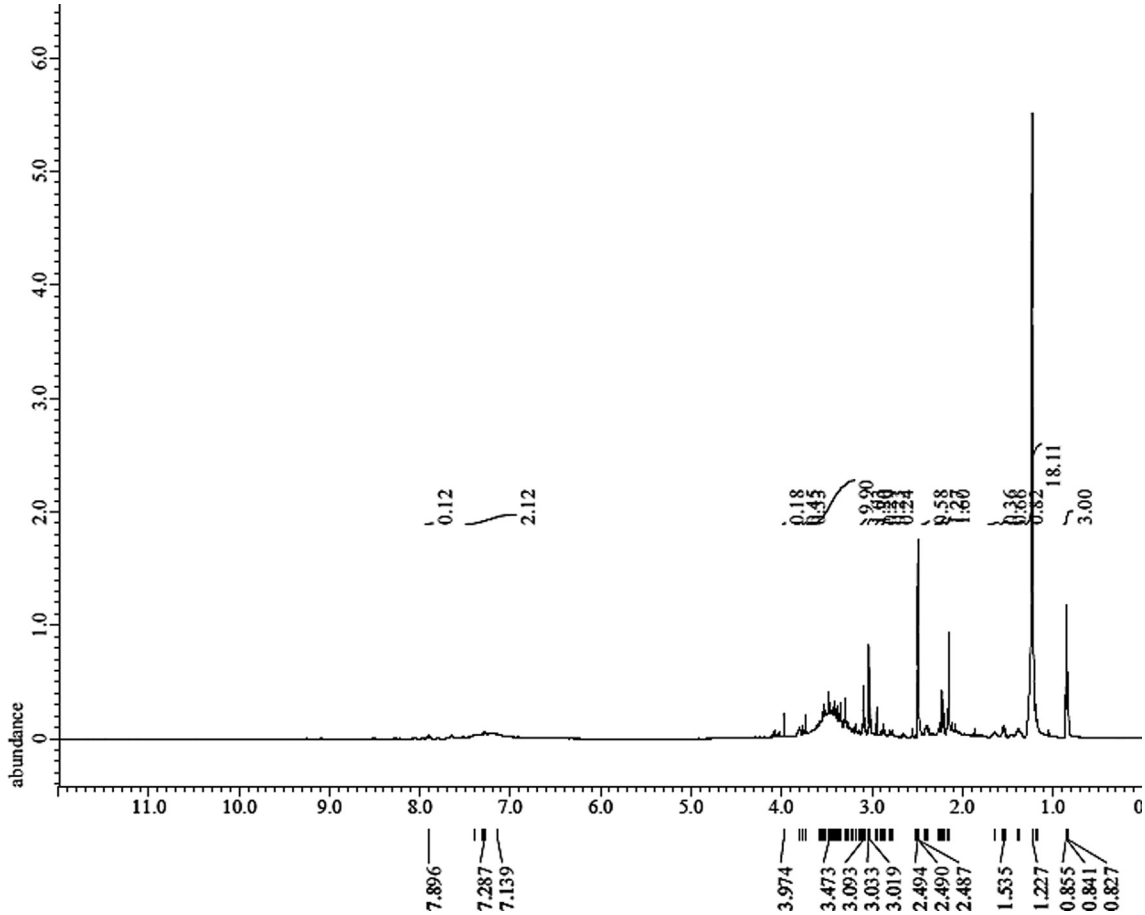

Fig. 4. [1]HNMR of CSII.

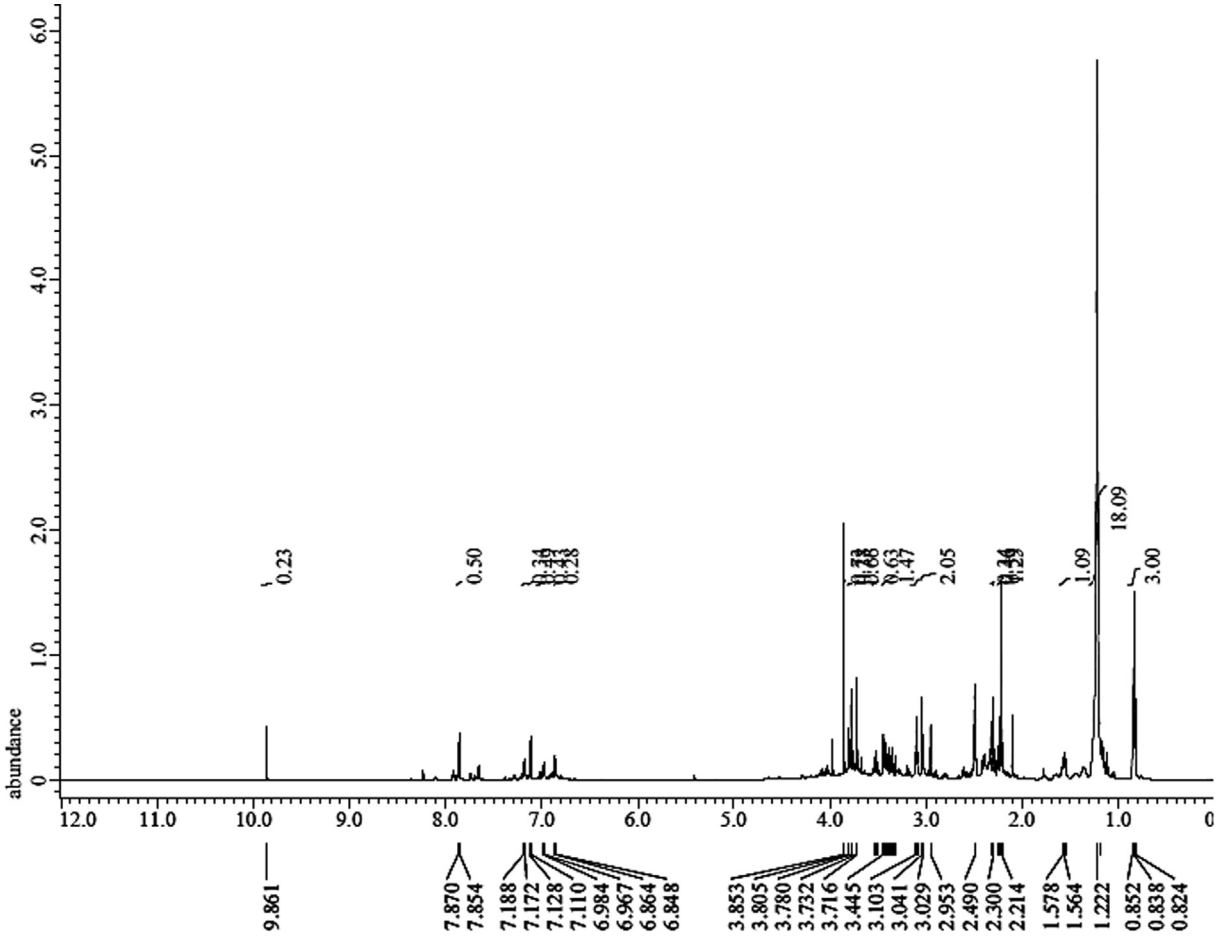

Fig. 5. ^{1}HNMR of CSIII.

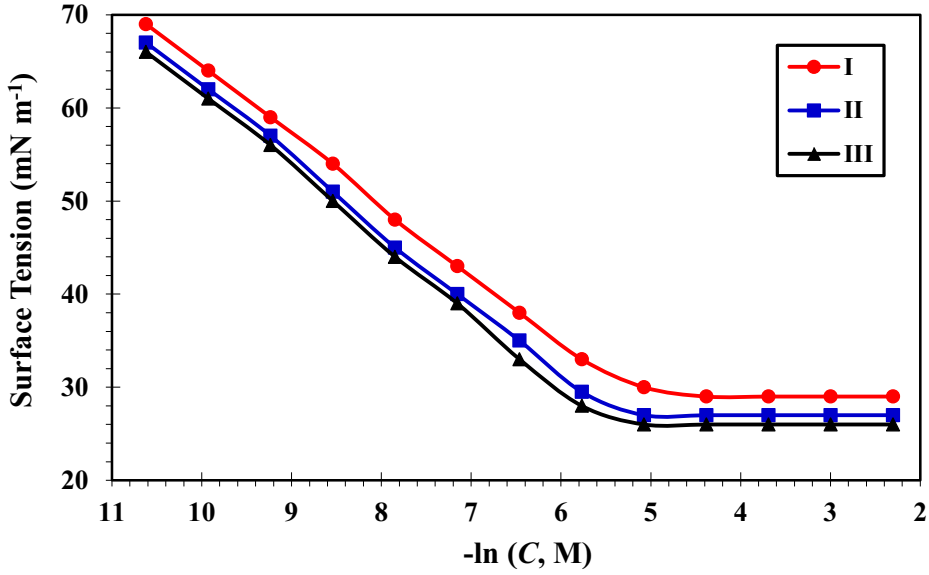

Fig. 6. Curve of surface tension (γ) against logarithm concentration (ln *C*) of the CSI, CSII & CSIII.

Table 1
Surface tension parameters of di-cationic surfactants in double distilled water at 25 °C.

Inhibitor	$C_{cmc} \times 10^3$ (M)	γ_{cmc} (mN m^{-1})	π_{cmc} (mN m^{-1})	$\Gamma_{max} \times 10^{10}$ (mol cm^{-2})	A_{min} (nm^2)
CSI	4.95	29	42	1.01	1.65
CSII	4.02	27	45	1.05	1.58
CSIII	3.91	27	46	1.07	1.55

Table 2
Weight loss data for CS in 1 M HCl in the absence and presence of different concentrations of di-cationic surfactants at different temperatures.

Inh. name	Inh. conc. (M)	25 °C			40 °C			55 °C			70 °C		
		k (mg cm^{-2}h^{-1})	θ	η_w (%)	k (mg cm^{-2}h^{-1})	θ	η_w (%)	k (mg cm^{-2}h^{-1})	θ	η_w (%)	k (mg cm^{-2}h^{-1})	θ	η_w (%)
Abs.	0	0.5304	–	–	1.1676	–	–	2.2146	–	–	4.0294	–	–
CSI	5×10^{-5}	0.0781	0.85	85.27	0.2298	0.80	80.32	0.4804	0.78	78.31	1.0104	0.75	74.92
	1×10^{-4}	0.0535	0.90	89.91	0.1571	0.87	86.54	0.3583	0.84	83.82	0.8790	0.78	78.19
	5×10^{-4}	0.0330	0.94	93.78	0.0986	0.92	91.56	0.2602	0.88	88.25	0.6330	0.84	84.29
	1×10^{-3}	0.0248	0.95	95.33	0.0860	0.93	92.63	0.2088	0.91	90.57	0.5208	0.87	87.07
CSII	5×10^{-5}	0.0739	0.86	86.07	0.2037	0.83	82.55	0.4570	0.79	79.37	0.9387	0.77	76.70
	1×10^{-4}	0.0488	0.91	90.80	0.1423	0.88	87.82	0.3498	0.84	84.20	0.7562	0.81	81.23
	5×10^{-4}	0.0304	0.94	94.27	0.0918	0.92	92.14	0.2375	0.89	89.28	0.5588	0.86	86.13
	1×10^{-3}	0.0217	0.96	95.91	0.0729	0.94	93.76	0.1908	0.91	91.39	0.4344	0.89	89.22
CSIII	5×10^{-5}	0.0704	0.87	86.72	0.1824	0.84	84.38	0.3954	0.82	82.14	0.7996	0.80	80.16
	1×10^{-4}	0.0404	0.92	92.38	0.1045	0.91	91.05	0.2852	0.87	87.12	0.5854	0.85	85.47
	5×10^{-4}	0.0265	0.95	95.00	0.0804	0.93	93.11	0.1947	0.91	91.21	0.4625	0.89	88.52
	1×10^{-3}	0.0203	0.96	96.18	0.0556	0.95	95.24	0.1456	0.93	93.42	0.3591	0.91	91.09

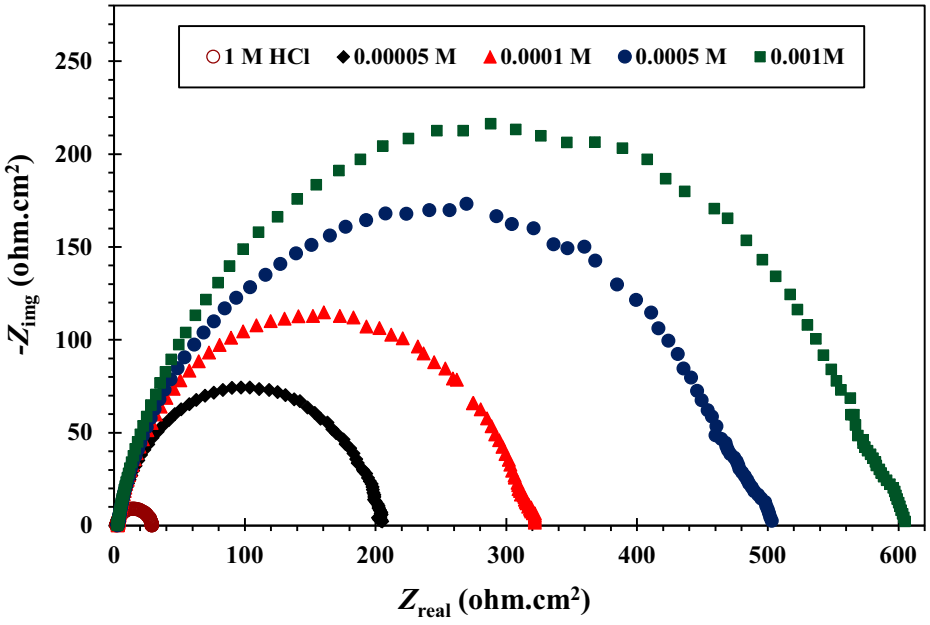

Fig. 7. Nyquist plot for CS in 1 M HCl in existence and absenteeism of varied concentrations of CSIII.

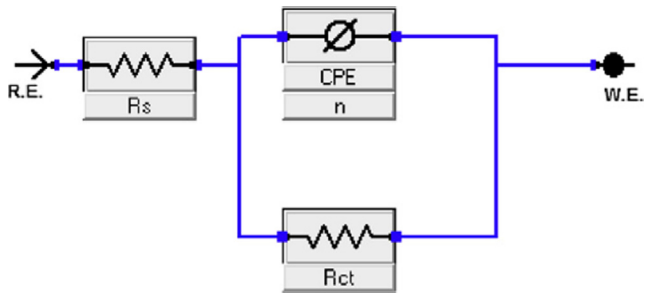

Fig. 8. Equivalent circuit used to pattern impedance measurements calculated for CS in 1 M HCl in existence and absenteeism of varied concentrations of CSI, CSII & CSIII.

3.2. Surface tension

Surface tension (γ) reductions linearly with augmentation of concentration ($-\ln C$) of CSI, CSII & CSIII until C_{cmc} Then stability occurs after that as in Fig. 6. The existence of surfactants in medium provide us with data about effectiveness (π_{cmc}), area/molecule at an air–water interface (A_{min}), and surface excess concentration (T_{max}) of CSI, CSII & CSIII. C_{cmc} data gained from the breakpoint of $\gamma - \ln C$ curve as in Table 1. By comparison, C_{cmc} for the three CSI, CSII & CSIII, it was observed that the increment in hydrophobicity of dicationic surfactants molecules leading to lowering C_{cmc} values. This is attributed to 4-methoxy benzyl > cinnamyl > furanyl according to the total hydrophobicity. Therefore, CSI, CSII & CSIII

Table 3
EIS parameters for CS corrosion in 1 M HCl in the absence and presence of different concentrations of di-cationic surfactants at 25° C.

Inhibitor name	Tested Solution	R_s (Ω cm^2)	Q_{dl} (mΩ^{-1} s^n cm^{-2})	n	R_{ct} (Ω cm^2)	C_{dl} (μF cm^{-2})	*Chi-sq*	η_I (%)
Absence	1 M HCl	2.06	0.3595	0.85	26.22	64.51	0.00353	–
CSI	5×10^{-5}	2.27	0.0575	0.90	165.7	10.34	0.00476	84.18
	1×10^{-4}	2.18	0.0455	0.88	234.3	8.27	0.00198	88.81
	5×10^{-4}	1.92	0.0309	0.87	370.6	5.07	0.00345	92.92
	1×10^{-3}	2.00	0.0207	0.87	490.0	4.33	0.00315	94.65
CSII	5×10^{-5}	2.79	0.0392	0.89	183.7	9.17	0.00338	85.73
	1×10^{-4}	2.83	0.0383	0.87	262.4	7.07	0.00129	90.01
	5×10^{-4}	2.45	0.0239	0.85	407.9	4.37	0.00133	93.57
	1×10^{-3}	2.82	0.0196	0.87	522.9	3.77	0.00298	94.99
CSIII	5×10^{-5}	2.99	0.0494	0.87	195.0	9.01	0.00330	86.55
	1×10^{-4}	3.01	0.0373	0.87	306.3	6.12	0.00161	91.44
	5×10^{-4}	2.97	0.0213	0.85	472.8	4.08	0.00133	94.45
	1×10^{-3}	3.07	0.0177	0.87	575.5	3.36	0.00313	95.44

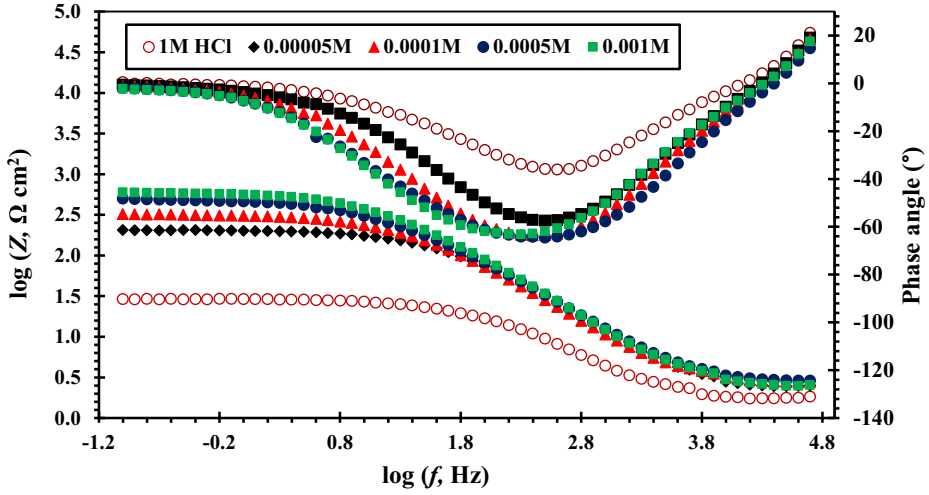

Fig. 9. Bode and Phase angle curve for CS in 1 M HCl in existence and absenteeism of various concentrations of CSIII.

gather into masses, where the hydrophilic group is pointed across water while the hydrophobic group is pointed towards the inside to form a micelle to obviate a relate with an aqueous medium, that way lowering the free energy of the structure. Subsequently, by augmentation hydrophobic group numbers, the tendency of the surfactants to form micelle augments, consequently C_{cmc} decreases [21].

Effectiveness (π_{cmc}) of CSI, CSII & CSIII can be evaluated by the following eq. [22] and listed in Table 1:

$$\pi_{cmc} = \gamma_o - \gamma \quad (1)$$

where γ_o & γ is surface tension of DW & of CSI, CSII & CSIII solution at C_{cmc}, respectively.

Besides, Table 1 records the surface pressure values of cationic surfactants (π_{cmc}). It is evident that the effectiveness values (π_{cmc}) augment with augmentation of a hydrophobicity of surfactants in aqueous media.

T_{max} at the link was evaluated from the following eq. [23]:

$$T_{max} = \frac{1}{nRT}\left(\frac{d\gamma}{dlnC}\right) \quad (2)$$

where $d\gamma/\mathrm{d}\ln C$ is a slope of straight line before C_{cmc} of (γ *vs.* $-\ln C$) plot and n is no. of species ions in a liquid phase.

T_{max} value decreases according to the follows order: CSIII > CSII > CSI. T_{max} augments because of increment in hydrophobicity structure of CSI, CSII & CSIII in solution.

Besides, the A_{min} was evaluated from the next eq. [24]:

$$A_{min} = \frac{10^{14}}{N_A T_{max}} \quad (3)$$

where N_A is Avogadro's no.

The values of (A_{min}) were evaluated and recorded in Table 1. It observed that A_{min} value decreases according to the following order: CSI > CSII > CSIII. A_{min} value decreases because of increment in hydrophobicity structure of CSI, CSII & CSIII in solution.

3.3. Weight loss measurements

Weight loss datum of CS in 1 M HCl in existence & absenteeism of varied concentrations of CSI, CSII & CSIII were calculated. Then calculate the inhibition efficiency (η_w) as following eq. [25]:

$$\eta_w = \left(\frac{W_{corr} - W_{corr(inh)}}{W_{corr}}\right) \times 100 \quad (4)$$

where W_{corr} and $W_{corr(inh)}$ are the weight loss of CS with and without the CSI, CSII & CSIII.

The results offer that η_w of the CSI, CSII & CSIII increases with augmentation of CSI, CSII & CSIII concentration. This behavior is because of surface encasement through adsorption of CSI, CSII & CSIII.

Effectiveness of heat on CS in the heat range 25–70 °C in corrosive medium in occurrence and absenteeism of various concentrations of the CSI, CSII & CSIII were accomplished by weight loss technique and shown in (**Supplementary materials,** Figs. 10–12)

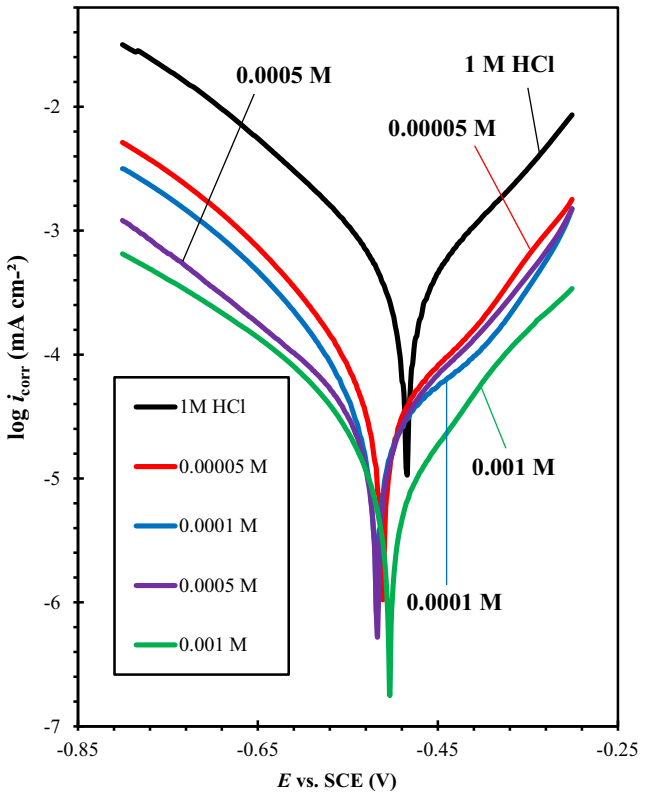

Fig. 10. Tafel polarization plot for CS gained at 25 °C in 1 M HCl solution in existence and absenteeism of varied concentrations of CSII.

and recorded in Table 2. Data demonstration that η_w slightly decreases in the following range 25–70 °C. This refers to protection of CSI, CSII & CSIII to CS face in tested medium maybe tend to chemical adsorption than physical adsorption.

3.4. Impedance results

The deterioration performance of CS in tested medium in occurrence and absenteeism of diversified concentrations of CSI, CSII & CSIII is assay by EIS at 25 °C. Fig. 7 **&** (**Supplementary materials,** Figs. 13 and 14) show Nyquist curves of CS in tested medium in occurrence & absenteeism of distinct concentrations of CSI, CSII & CSIII. Nyquist curves exhibit one capacitive semi-circle. A capacitive loop referred that a suppression of CS in a tested medium under control by the charge transfer operation. And CSI, CSII & CSIII form barrier film on CS face in existence of CSI, CSII & CSIII. The variation in the actual impedance, at low and high frequencies, it looked as the polarization resistance (R_P) [26]. R_P includes the resistance of cumulative kinds, the charges transfer resistance (R_{ct}), and the diffuse layer resistance (R_d). It is established that R_{ct} increases in existence of CSI, CSII & CSIII further than in absenteeism of them. R_{ct} increases as concentration increased. The increment in R_{ct} is concerning with a slower destroying system, due to reducing the activated centers, which are needful for the corrosion reaction. However, *CPE* used instead of pure capacitance (C_{dl}). EIS spectrum is supplied with a convenient equivalent circuit as Fig. 8. The equivalent circuit consists of R_s, R_{ct} and *CPE* (constant phase element) instead of C_{dl}.

The C_{dl} values determined by the next formula:

$$Cdl = Q_{dl}(\omega max)^{n-1} \tag{5}$$

Impedance (ZCPE) is calculated by the following equation:

$$Z_{CPE} = Q_{dl}^{-1}(i\omega_{max}) - n \tag{6}$$

$$\omega = 2\pi f_{max} \tag{7}$$

where Q_{dl}, ω max, f_{max}, i, n are constant phase element, the angular frequency, the frequency at a maximum imaginary element of the impedance, an imaginary number, and a coefficient of surface inhomogeneity, respectively.

EIS variables were evaluated by the equivalent circuit. Table 3 clears that n values are 0.5 to 1, which refers that the adsorption barrier is considered a capacitive double layer. As shown in Table 3, C_{dl} values decrease as the CSI, CSII & CSIII concentration increase. The C_{dl} is decreased because the water molecules are replaced by CSI, CSII & CSIII on CS surface. Therefore C_{dl} value is smallest in existence of CSI, CSII & CSIII than in them absenteeism. The adsorption of CSI, CSII & CSIII maybe raises thickness of the double layer agreeing to Helmholtz pattern [27]. Bode and Phase curves for CS in tested medium in absenteeism and existence of CSI, CSII & CSIII are shown in Fig. 9 **&** (**Supplementary materials,** Figs. 15 and 16). It was established that the impedance value augments with increment of CSI, CSII & CSIII concentration. Forming of a covering layer of CSI, CSII & CSIII on a metal face prohibits the degradation of iron in an acidic medium.

The inhibition efficiency (η_I) is evaluated according to the next eq. [28,29]:

$$\eta_I = \left(\frac{R_{ct}(inh) - R_{ct}}{R_{ct}(inh)}\right) \times 100 \tag{8}$$

where R_{ct} and $R_{ct}(inh)$ are the charge transfer resistance in occurrence and absenteeism of various concentrations CSI, CSII & CSIII.

η_I was recorded in Table 3; and as in Table 3 the inhibition efficiency (η_I) augments as CSI, CSII & CSIII concentration increase.

Table 4
Tafel polarization parameters for CS corrosion in 1 M HCl in the absence and presence of different concentrations of di-cationic surfactants at 25 °C.

Inhibitor	Conc. of inhibitor (M)	E_{corr} V(SCE)	i_{corr} (mA cm^{-2})	β_a (V dec^{-1})	β_c (V dec^{-1})	η_p (%)
Absence	0	−0.484	0.5465	0.152	−0.164	–
CSI	5×10^{-5}	−0.529	0.0849	0.168	−0.182	84.46
	1×10^{-4}	−0.496	0.0615	0.180	−0.159	88.75
	5×10^{-4}	−0.514	0.0375	0.155	−0.168	93.14
	1×10^{-3}	−0.519	0.0277	0.176	−0.206	94.94
CSII	5×10^{-5}	−0.511	0.0800	0.165	−0.144	85.36
	1×10^{-4}	−0.519	0.0589	0.185	−0.146	89.22
	5×10^{-4}	−0.517	0.0330	0.145	−0.178	93.96
	1×10^{-3}	−0.504	0.0264	0.187	−0.204	95.16
CSIII	5×10^{-5}	−0.531	0.0781	0.141	−0.141	85.71
	1×10^{-4}	−0.521	0.0462	0.174	−0.177	91.55
	5×10^{-4}	−0.505	0.0295	0.178	−0.175	94.60
	1×10^{-3}	−0.539	0.0247	0.108	−0.139	95.49

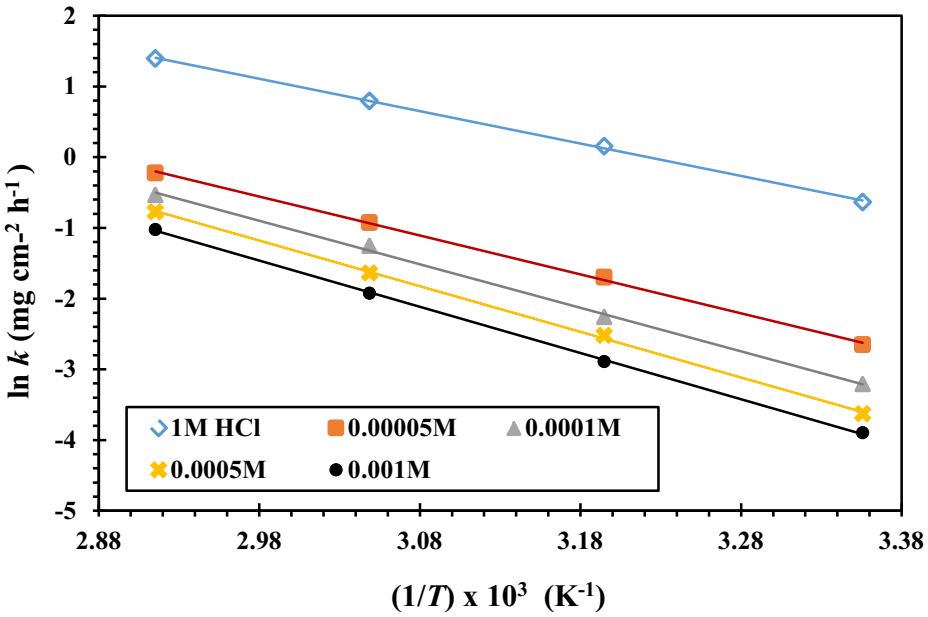

Fig. 11. Arrhenius plot (ln k vs. $1/T$) for CS degradation in existence and absenteeism of various concentrations of CSIII in 1 M HCl medium.

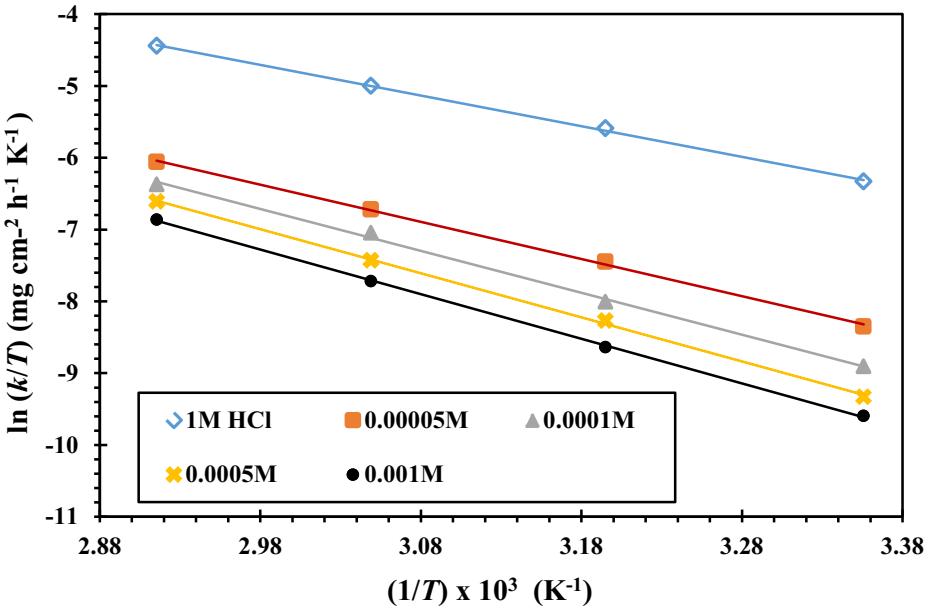

Fig. 12. Transition-state plot (ln k/T vs. $1/T$) for CS degradation in existence and absenteeism of varied concentrations of CSIII in 1 M HCl solution.

Table 5
Activation parameters for CS in 1 M HCl in the absence and presence of different concentrations of di-cationic surfactants.

Inhibitor name	Conc. of inhibitor (M)	E_a (kJ mol^{-1})	ΔH^* (kJ mol^{-1})	- ΔS^* (J mol^{-1} K^{-1})
Absence	0	38.14	35.49	130.33
CSI	5×10^{-5}	47.80	45.15	113.52
	1×10^{-4}	52.26	49.61	102.04
	5×10^{-4}	55.75	53.09	102.04
	1×10^{-3}	56.88	54.23	94.45
CSII	5×10^{-5}	47.88	35.49	113.91
	1×10^{-4}	51.77	45.22	104.35
	5×10^{-4}	54.94	49.11	97.76
	1×10^{-3}	56.51	52.28	94.99
CSIII	5×10^{-5}	45.75	43.10	121.52
	1×10^{-4}	51.17	48.52	108.19
	5×10^{-4}	53.65	51.00	103.14
	1×10^{-3}	54.31	51.66	103.54

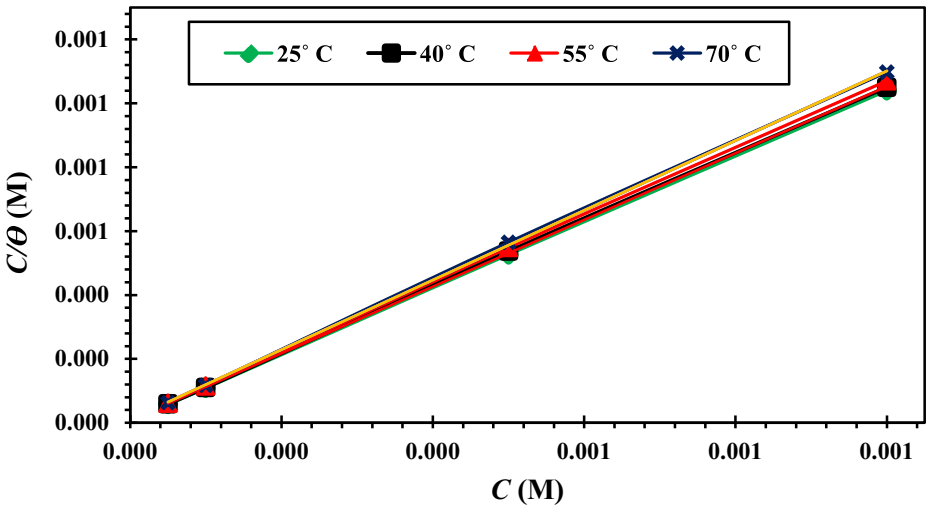

Fig. 13. Langmuir isotherm adsorption pattern of CSIII on CS face in 1 M HCl at varied temperatures.

Table 6
Standard thermodynamic parameters of adsorption on carbon steel surface in 1 M HCl containing different concentrations of di-cationic surfactants.

Inhibitors name	Temp. (C)	K_{ads} (M^{-1})	$\triangle G^{o}_{ads}$ (kJ mol^{-1})	$\triangle H^{o}_{ads}$ (kJ mol^{-1})	$\triangle S^{o}_{ads}$ (J mol^{-1} K^{-1})
CSI	25	129,154	− 39.11	− 11.84	91.51
	40	111,517	− 40.70		92.19
	55	88,449	− 42.01		91.99
	70	69,245	− 43.24		91.54
CSII	25	133,523	− 39.19	− 11.37	93.36
	40	113,230	− 40.73		93.82
	55	90,659	− 42.08		93.63
	70	73,491	− 43.41		93.41
CSIII	25	163,757	− 39.70	− 9.99	99.67
	40	125,595	− 41.00		99.07
	55	101,811	− 42.40		98.79
	70	98,161	− 44.23		99.82

3.5. Potentiodynamic polarization

Fig. 10 **&** (**Supplementary materials,** Figs. 17 and 18) show Tafel plots for CS in tested medium at several concentrations of CSI, CSII & CSIII at 25 °C. The deterioration current densities (i_{corr}), deterioration potential (E_{corr}), cathodic Tafel slope (β_c), and anodic Tafel slope (β_a) which gained are recorded in Table 4. It evident that the (i_{corr}) minifies with increment of CSI, CSII & CSIII concentration. The existence of the CSI, CSII & CSIII gave a little movement of the (E_{corr}) in a positive way. So the CSI, CSII & CSIII were considered a mixed inhibitor [30]. Besides, (β_a andβ_c) are lightly changed with increment of the CSI, CSII & CSIII concentration. This means that CSI, CSII & CSIII prevent deterioration by deactivation of active sites without change the deterioration mechanism. The anodic and cathodic Tafel lines are moved a little to deterioration current densities. This is due to inhibition activity of CSI, CSII & CSIII executes by deactivation of active sites of CS face and reduces the surface region susceptible to the damage [31].

The (η_p) was evaluated from the following eq. [32]:

$$\eta_p = \frac{i_{corr} - i_{corr}(inh)}{i_{corr}} \times 100 \quad (9)$$

where i_{corr} & i_{corr}(inh) are deterioration current densities in occurrence & absenteeism of various concentrations of CSI, CSII & CSIII concentration.

The values of the (η_p) is recorded in Table 4. η_p augments with augmentation of CSI, CSII & CSIII concentration.

3.6. Dissolution parameters

Activation energy (E_a) values are evaluated from Arrhenius equation as follows [33]:

$$k = Aexp\left(\frac{-E_a}{RT}\right) \quad (10)$$

Enthalpy (ΔH^*) & entropy (ΔS^*) of activation are evaluated from Wine–Jones–Erying equation [34]:

$$ln\left(\frac{k}{T}\right) = \left(ln\left(\frac{R}{N_A h}\right) + \left(\frac{\Delta S^*}{R}\right)\right) - \frac{\Delta H^*}{RT} \quad (11)$$

where k is deterioration rate, A is frequency factor, T is absolute temp., R and h are universal gas and Planck's constants and N_A is Avogadro's no.

Arrhenius plots ($\ln k$ *vs.* $1/T$) for CS dissolution in occurrence and absenteeism of various concentrations of CSI, CSII & CSIII in 1 M HCl solution is presented in Fig. 11 & (**Supplementary materials, Figs. 19 and 20**). Slope of straight lines $= -E_a/R$. E_a values in the presence of CSI, CSII & CSIII are slightly bigger than that obtained in HCl solution. This indicates that CSI, CSII & CSIII adsorption on CS is physical and chemical**.**

Fig. 12 & (**Supplementary materials, Figs. 21 and 22**) represent Transition-state curves ($\ln k/T$ *vs.* $1/T$) for CS dissolution in occurrence and absenteeism of various concentrations of CSI, CSII & CSIII in 1 M HCl solution. Slope of straight lines $= -\Delta H^*/R$ and the intercept $= \ln(R/N_A h) + (\Delta S^*/R)$. $E_a, \Delta H^*$ and ΔS^* values are recorded in Table 5. The +ve signs of (ΔH^*) refer to an endother-

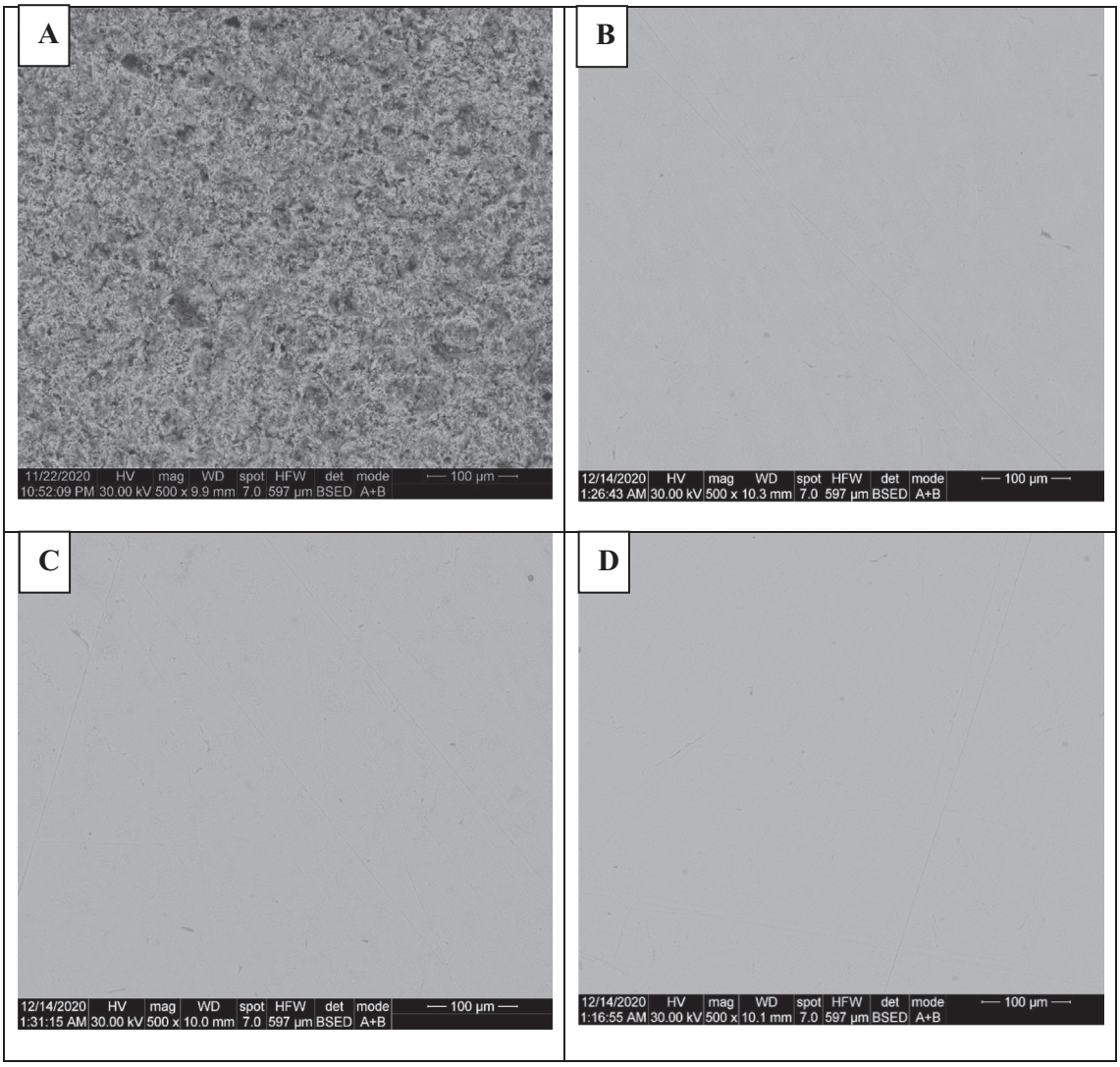

Fig. 14. SEM graphs of CS surface in existence and absenteeism of 1×10^{-3}M of CSI, CSII & CSIII for one day at room temperature.

mic of CS dissolution reaction and refer that the degradation of CS is hard [35]. Activation entropy (ΔS^{*}) has a negative sign. This indicates that the association rather than dissociation of activated complex [36].

3.7. Adsorption isotherm

CSI, CSII & CSIII prohibit a suppression of CS by adsorption on a steel – medium link. Adsorption supplies information about interlink between adsorbed molecules and electrode face. A grade of surface covering (θ) for varying concentrations of the CSI, CSII & CSIII in corrosive media has been calculated from the following eq. [37]:

$$\theta = \left(\frac{W_{corr} - W_{corr(inh)}}{W_{corr}}\right) \quad (12)$$

where W_{corr} and $W_{corr(inh)}$ are the weight loss of CS with and without the CSI, CSII & CSIII.

Langmiur isotherm using equilibrium const. (K_{ads}) characterizes in the equation [38,39]:

$$\frac{C}{\theta} = \frac{1}{K_{ads}} + C \quad (13)$$

where C is the CSI, CSII & CSIII concentration.

Curve of C/θ against C Fig. 13 & (**Supplementary materials, Figs. 23 and 24**) produces a rectum line with slope equivalent unity. This approves the adsorption of the CSI, CSII & CSIII on the CS surface track the Langmuir isotherm**.**

Standard free energy of adsorption (ΔG^{o}_{ads}) evaluates as the following eq. [40]:

$$\Delta G^{o}_{ads} = -RTln(55.5K_{ads}) \quad (14)$$

where K_{ads} is equilibrium const. of CSI, CSII & CSIII adsorption process.

Negative values of ΔG^{o}_{ads}denotes that the interaction of CSI, CSII & CSIII on CS face in 1 M HCl is an instant reaction. When ΔG^{o}_{ads} values $\leq$ -20 kJ/mol refers to physical interlinkage between the CSI, CSII & CSIII molecules and the charged CS surface. ΔG^{o}_{ads} values $\geq -$ 40 kJ/mol refers to coordination bond of CSI, CSII & CSIII molecules and CS surface (chemisorption) [41]. ΔG^{o}_{ads}values are −39.11, − 40.70, − 42,01 and − 43.24 kJ/mol for **CSI**, −39.19, − 40.73, 42,08 and − 43.41 kJ/mol for **CSII** , −39.70, − 41.00, − 42.40 and − 44,23 for **CSIII** at 25, 40, 55 and 70 °C, respectively. These values indicate CSI, CSII & CSIII molecules adsorbed on CS through physical and chemical bond [42]. Great ΔG^{o}_{ads} values &

their -ve signs are referring to a powerful interlinkage and extremely effective adsorption [43].

ΔH^{o}_{ads} is estimated agreeing to the equation of Van't Hoff [22,29]:

$$lnK_{ads} = \left(\frac{-\Delta H^{o}_{ads}}{RT}\right) + \text{constant} \quad (15)$$

ΔH^{o}_{ads} values are −11.84 kJ/mol for CSI, −11.37 kJ/mol for CSII & −9.99 for CSIII. These values indicate CSI, CSII & CSIII molecules adsorbed on CS through exothermic reaction [44].

ΔS^{o}_{ads} was calculated from the basic thermodynamic equation [45]:

$$\Delta G^{o}_{ads} = \Delta H^{o}_{ads} - T\Delta S^{o}_{ads} \quad (16)$$

The positive ΔS^{o}_{ads} values indicate the natural adsorptive ability of CSI, CSII & CSIII molecules on CS surface [46].

The ΔG^{o}_{ads}, ΔH^{o}_{ads}, ΔH^{o}_{ads} parameters of CSI, CSII & CSIII adsorption at several concentrations and temperatures on MS face in 1 M HCl are given in Table 6.

3.8. Scanning electron microscopy (SEM)

SEM studies are executed to examine if the corrosion inhibition of CS specimens occurs due forming of a covering layer on a surface or not. Fig. 14 shows SEM graphs of CS surface in occurrence and absenteeism of 1x10^{-3}M of CSI, CSII & CSIII for one day at room temperature. In the absenteeism of CSI, CSII & CSIII, the damages and corroding figure were apparent. But, in the presence of CSI, CSII & CSIII, the smooth and protected surface are present. Furthermore, SEM photo confirmed the chemical and electrochemical results.

3.9. Atomic force microscope (AFM)

AFM microscope graphs of CS surface after immersing for one day without and with 1 × 10^{-3}M of CSI, CSII & CSIII at 25 °C are displayed in Fig. 15. In a blank sample, the damages and corroding were apparent. Also, high average roughness (R_a) values (124.0 nm) in absenteeism CSI, CSII & CSIII might be concerned to the corrosive species forming on CS substrate during immersed in corrosive medium. However, these injuries vanished remarkably after the addition of 1x10^{-3}M of CSI, CSII & CSIII in a corrosive environment. The variations of R_a were mitigated to lower values (23.1 nm, 19.0, and 17.5 nm) for CSI, CSII & CSIII, respectively). Additionally, it suggested that the ranking agrees to inhibitory performance of di-cationic surfactants (**CSIII > CSII > CSI**) which could protect the CS from corrosion [47,48].

3.10. Quantum chemical calculations

It was established experimentally that the carbon steel inhibition by di-cationic surfactants as inhibitors for the corrosion is in order:

CSIII > CSII > CSI

It was discovered that the explored inhibitor with methoxy benzylidene stray has higher restraint effectiveness than that with phenyallylidene and furan-2-ylmethylene groups on a metal face. The highest hindrance efficacy of **CSIII** than different inhibitors has likely alluded to an expanding number of centers of adsorption

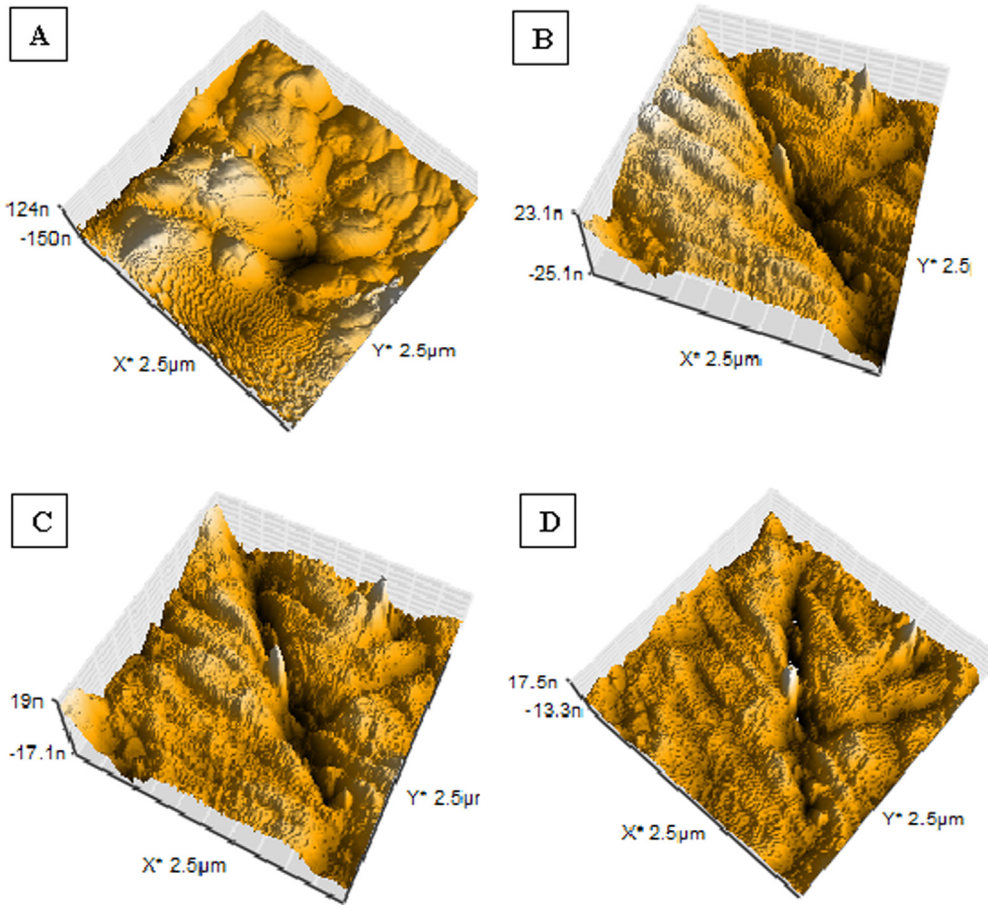

Fig. 15. AFM photo of (a) without inhibitor, (b) with CSI, (c) with CSII, and (d) with CSIII.

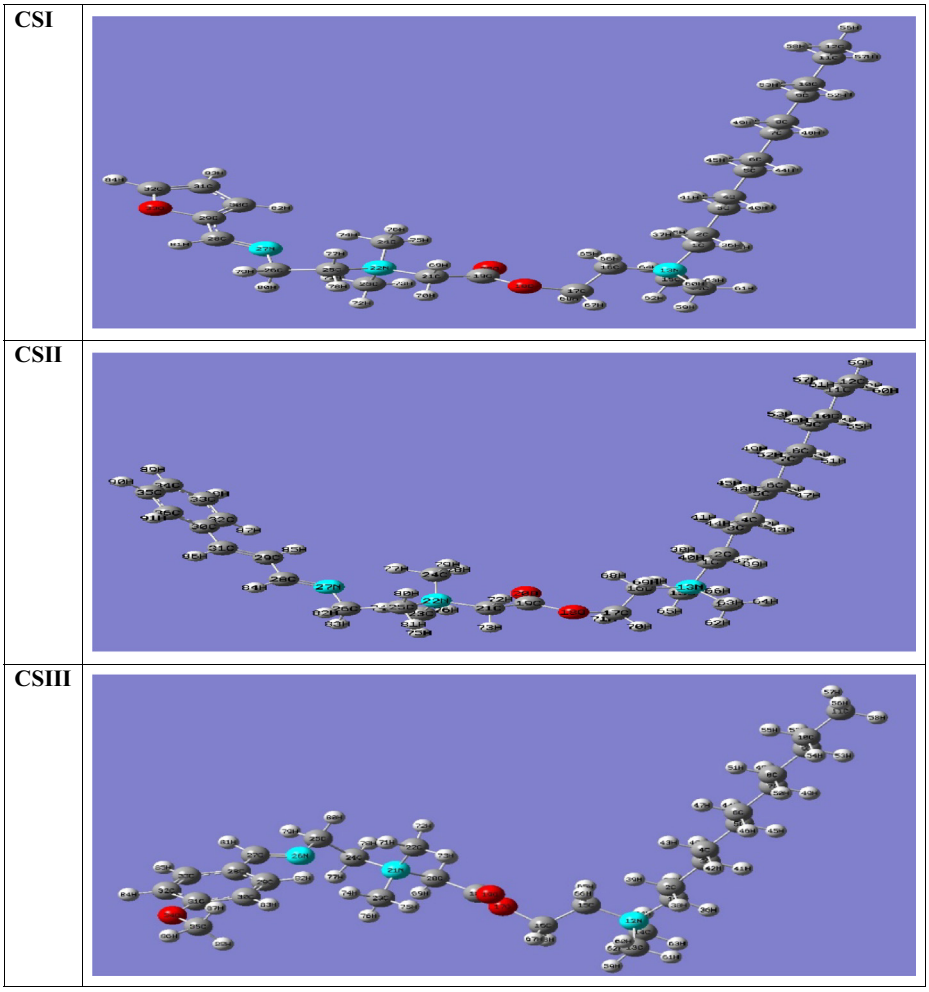

Fig. 16. Geometrical structure of: (a) CSI, (b) CSII, and (c) CSIII di-cationic surfactants obtained from computational conformation simulation.

Table 7
The calculated quantum chemical parameters obtained from DFT/6-31G (d,p) calculations.

Molecule	HOMO (a.u)	LUMO (a.u)	$\triangle E$ (a.u)	*DM* (Debye)	η (a.u)	σ (a.u)$^{-1}$	μ (a.u)	χ (a.u)	ω	*TNC* (e)	E_t (a.u.)	Volume (cm^3/mol)
CSI	−0.357	−0.256	0.123	27.441	0.062	16.129	0.317	−0.317	0.810	−7.976	1448.531	697.980
CSII	−0.357	−0.253	0.104	27.424	0.052	19.231	0.305	−0.305	0.894	−8.118	1528.165	795.167
CSIII	−0.353	−0.255	0.098	23.091	0.049	20.408	0.304	−0.304	0.943	−8.503	1525.957	809.158

on the inhibitors and the greater electron densities brought about by an electron liberation methoxy strays.

In like manner, quantum mechanics computations were executed to research the impact of parameters of the structures on the efficacy of surfactants and explore their mechanism of adsorption on a metal face. The molecular and electronic properties of the di-cationic surfactants were determined by enhancement of their bond lengths, angles, and distortion angles. A calculated structures with the least energies got from the computations are exhibited in Fig. 16.

As indicated by Koopman's hypothesis [49] E_{HOMO}andE_{LUMO} of the inhibitor particle are identified with theionizationpotential(I), andtheelectronaffinity(A), respectively other quantum variables that exhibit significant data about a reactivity of the di-cationic surfactants, are electronegativity(χ), chemicalpotential(μ), hardness(η)and softness(σ)are determined by:

$$I = -E_{HOMO} \tag{17}$$

$$A = -E_{LUMO} \tag{18}$$

$$\mu = -\chi \tag{19}$$

$$\mu = \frac{(E_{HOMO} + E_{LUMO})}{2} \tag{20}$$

$$\eta = \frac{(E_{LUMO} - E_{HOMO})}{2} \tag{21}$$

$$\sigma = \frac{1}{\eta} \tag{22}$$

Quantum variables acquired from computations which are liable to the hindrance of di-cationic surfactants, for example, the energies of HOMO and LUMO, gap energy betweenE_{LUMO} and E_{HOMO}, ΔE, addressing the reactivity, dipole moment(D), chemical potential (μ), electronegativity(χ), hardness(η), softness(σ), electrophilicity (ω), total negative charge

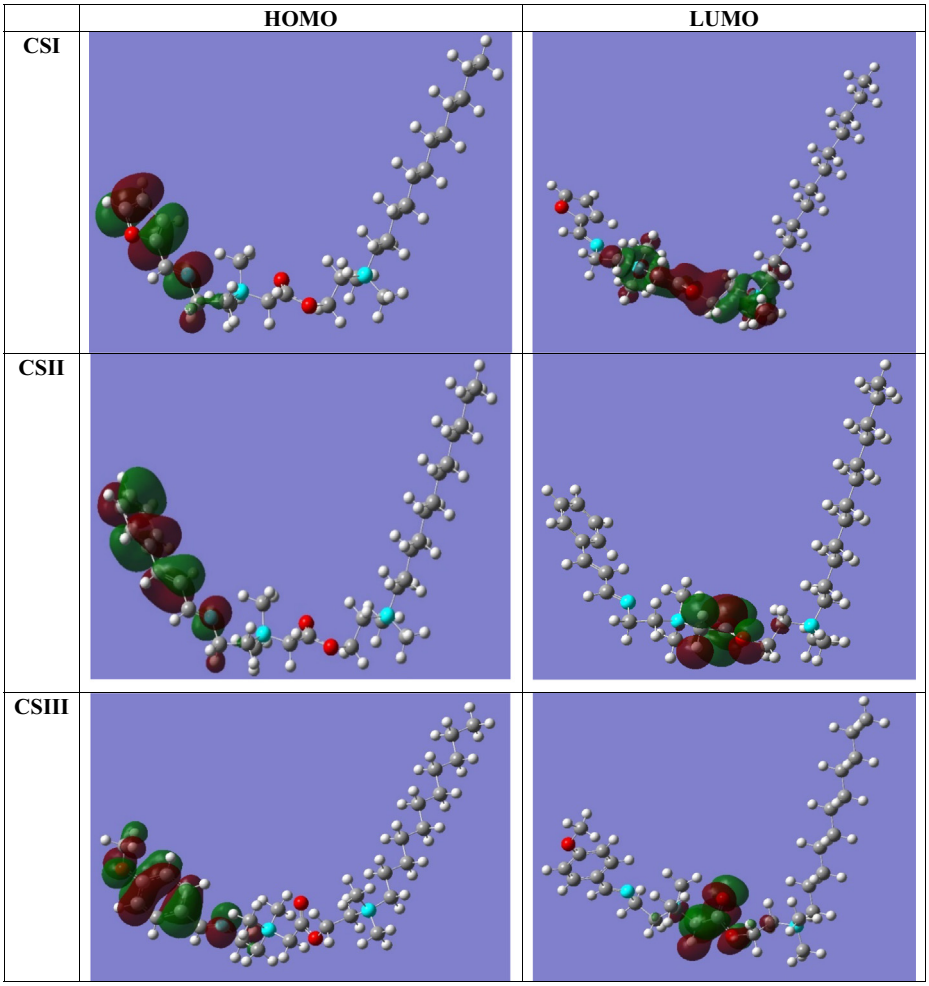

Fig. 17. The charge density distribution of (a) HOMO and (b) LUMO levels of the investigated di-cationic surfactants CSI, CSII, and CSIII.

(*TNC*)and total energy (E_t)are collected in Table 7. The surfactants may adsorb on a steel face as cation and portion of electrons betwixt the nitrogen in the surfactant and a metal face. Else chance is that a di-cationic surfactant may adsorb through electrostatic association betwixt positively charged surfactant and negatively charged steel face [50]. It has appeared from the study that the molecular structures of an explored surfactants are not planar, Fig. 16. According to the frontier orbital theory, substance reactivity is a parameter of the interactivity among the orbitals HOMOandLUMO of the responding kinds [51]. E_{HOMO} shows a capacity to give electrons to a convenient acceptor with virtual orbitals and E_{LUMO} demonstrates its capacity to admit electrons. The lower is the estimation of E_{LUMO}; the more is the capacity to admit electrons. The greater is an estimation of E_{HOMO} of a surfactant, the more prominent is its simplicity of presenting electrons to a vacant d-orbital of a steel face, and more noteworthy is its restraint productivity.

The computations demonstrated that CSIII has most noteworthy estimation of E_{HOMO} (−0.353 a.u) among the examined CSII and CSI, (−0.357 and −0.357 a.u.) respectively, Table 7. This could clarify the best inclination of CSIII inhibitors to adsorb on a metal face and likewise has the most noteworthy hindrance effectiveness. Appropriately, the request for expanding reactivity towards the surface will be: CSIII > CSII > CSI, which is in a decent concurrence with empirical remarks. HOMO – LUMO gap, ΔE, which is a remarkable evidence for stability, is exercised to create hypothetical patterns for clarifying the construction and adaptation hindrances in numerous structure frameworks. The smaller is the estimation of ΔE, the more likely that the matter has restraint proficiency [52,53]. It has appeared from the estimations that CSIII has a littlest HOMO – LUMO energy gap (0.098 a.u) contrasted and CSII and CSI (0.104 and 0.123 a.u.) respectively, Table 7. As needs be, it very well may be normal that CSIII has a wide tendency to adsorb on a metal face than different inhibitors which concurs well with the exploratory information. It was discovered that the variety of the determined LUMO energies among all examined surfactants hasn't corresponded with the restraint proficiency, Table 7.

The dipole second(D), the principal limb of the energy concerning exercised electric field, was utilized to talk about and support the construction [54]. There is a decent connection between's D and hindrance productivity. The particle with the most noteworthy productivity, CSIII, has the least dipole second, (23.091 D), Table 7. The sub-atomic volume is else quantum boundary got from the calculation data, Table 7. The slow expansion in the sub-atomic volumes of the surfactant particles suggests that a metal face territory covered by the particles is progressively expanded by expanding the hydrophobic chain length. This feedback is equal to the outcomes acquired from the polarization and impedance examines. It has appeared from the computations that the CSIII has the most elevated molecular volume with a worth equivalent 809.158 (cm^3/mol) contrasted with CSII and CSI (795.167 and 697.980 cm^3/mol), Table 7, which prompts increment its restraint productivity because of the expansion of the relate zone betwixt the particle and the metal face. In like manner, the expanding

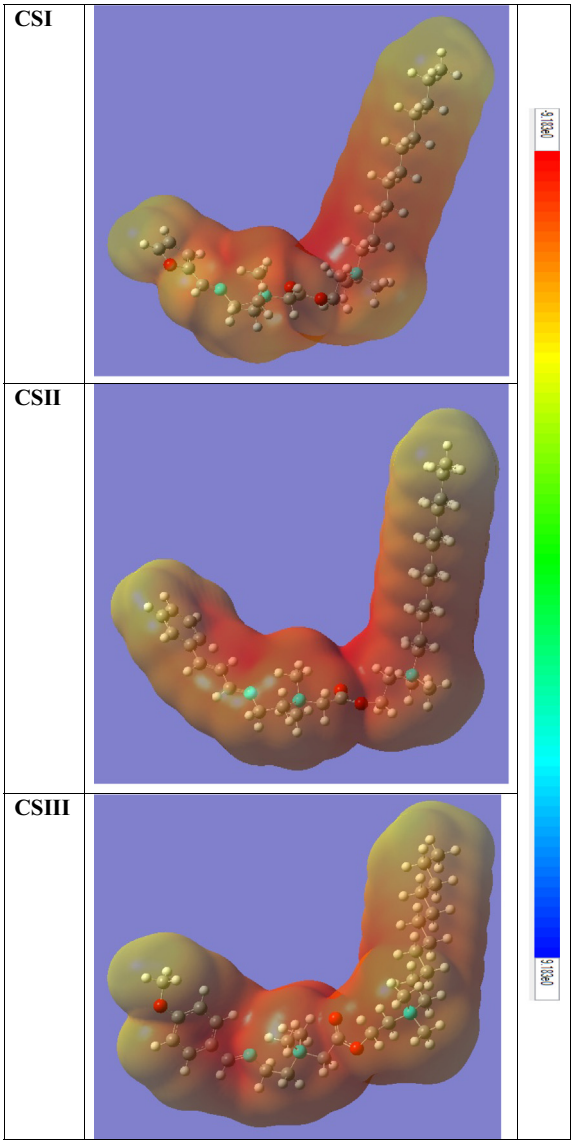

Fig. 18. Electron density plots of molecular electrostatic potentials (MEP) of CSI, CSII, and CSIII di-cationic surfactants.

reactivity will be: CSIII > CSII > CSI which is in a decent concurrence with the exploratory observations. An ultimate hardness and softness, η, σ, respectively, are significant properties that assess the reactivity and stability of a surfactant. A tough one possesses a huge ΔE and a soft one possesses a little ΔE. Hard compounds are very stable than soft matters since soft molecules could undoubtedly submit electrons to an acceptor. At least difficult exchange of electrons, adsorption could happen at a piece of an inhibitor where σ, possesses a greatest value [55]. In a corrosion system, a surfactant goes about as a Lewis base while a metal goes about as a Lewis corrosive, respectively. Bulk metals are delicate acids and hence delicate di-cationic surfactants are best for acidic corrosion of those metals. Likewise, it is presumed that CSIII with the most noteworthy σesteem (20.408 a.u^{-1}) has the most noteworthy capacity restraint effectiveness compared to CSII and CSI (19.231 and 16.129 a.u^{-1}) respectively, Table 7, which is in good harmony with the experimental data. Also, the computations exhibited that CSIII has a smallest $\chi$and has a largest $\omega$and *TNC* (−0.304 a.u., 0.943 and −8.503 e), respectively, Table 7, which drives to augmentation of its donation capability to a steel face and subsequently enhance its suppression efficacy. It is concluded from the above discussion that the optimized parameters confirm that the inhibitor with a high alkyl chain has the most efficiency which concurs well with the experimental data. On the other hand, HOMO level of all cationic surfactants is mostly centralized at the end of an alkyl chain, which exhibits that the hydrophobic stray is the favored locales for an electrophilic assault at a steel face, Fig. 17. This implies that an alkyl chain portion with great coefficients of HOMO charge density was arranged across a steel face and the adsorption most likely happens through the π−electrons of it. Additionally, calculations indicated that the charge density of the LUMO level is restricted on a center of a particle-containing (*N*) for all explored matters which implies that this portion could be responded to as electrophile (electron acceptor), Fig. 17.

The molecular electrostatic potentials are exceptionally useful in that negative districts may be viewed as nucleophilic centers, while areas with positive electrostatic potential will be potential electrophilic destinations. Besides, the electrostatic potential makes the polarization of the electron density obvious. The computations demonstrated that a hydrophobic chain and the nitrogen possess a negative electrostatic potential which implies that these locales are the dynamic sites for linking to a steel face, Fig. 18.

4. Mechanism of inhibition

Adsorption of organic molecules on solid faces may be physical or chemical or both adsorption. A physical adsorption takes place by electrostatic interlinkage betwixt charged metal face and charged inhibitor molecule [56]. A chemical adsorption takes place by interlinkage between free electron pairs of the heteroatoms and π-electrons of multiple bonds [57]. A steel surface in an acidic medium has a negative charge and a surfactant is positively charged so electrostatic attraction between a polar head group of a surfactant and a metal face is arising. Di-cationic surfactant has a big size and high molecular weight has greater inhibition efficiency [58].

The inhibition efficacy values of the examined di-cationic surfactants in1M HCl were in the following order: CSIII > CSII > CSI.

5. Conclusions

1. CSI, CSII & CSIII exhibit a perfect inhibitor for corrosion of CS in 1 M HCl.
2. Active surface properties of three CSI, CSII & CSIII such as their surface tension, C_{cmc}, and other parameters in 1 M HCl at 25 °C were specified and discussed.
3. Inhibition efficacy augments by augmenting concentration of CSI, CSII & CSIII but slightly increment in temperature of 25–70 °C.
4. Double layer capacitances minimize for blank solution compared to in the existence of CSI, CSII & CSIII. This fact may be demonstrated by adsorption of the CSI, CSII & CSIII on a metal face.
5. Tafel polarization plots refer that i_{corr} diminishes and E_{corr} changes a few with adding of the synthesized di-cationic surfactants, so the CSI, CSII & CSIII are a mixed kind.
6. Activation energy increases with an increment of the CSI, CSII & CSIII concentration.
7. Adsorption of CSI, CSII & CSIII on CS surface follow Langmuir isotherm and is mixed kind.
8. Both SEM and AFM techniques confirmed the forming of a good protective layer.

9. The computed quantum variables demonstrated a decent relation of those parameters for the explored di-cationic surfactants and their hindrance efficacy for the corrosion of CS.
10. Inhibition efficacy of di-cationic surfactants follows the order: CSIII > CSII > CSI.

Declaration of Competing Interest

The authors declare that they have no known competing financial interests or personal relationships that could have appeared to influence the work reported in this paper.

Appendix A. Supplementary material

Supplementary data to this article can be found online at https://doi.org/10.1016/j.molliq.2021.116541.

References

[1] P.B. Raja, A.K. Qureshi, A.A. Rahim, H. Osman, K. Awang, Corros. Sci. 69 (2013) 292–301.
[2] R. Solmaz, Corros. Sci. 79 (2014) 169–176.
[3] M. Tourabi, K. Nohair, M. Traisnel, C. Jama, F. Bentiss, Corros Sci. 75 (2013) 123–133.
[4] E.M.S. Azzam, M.A. Hegazy, N.G. Kandil, A.M. Badawi, R.M. Sami, Egypt. J. Petrol. 24 (2015) 493–503.
[5] O. Kaczerewska, R. Leiva-Garcia, R. Akid, B. Brycki, I. Kowalczyk, T. Pospieszny, J. Mol. Liq. 249 (2018) 1113–1124.
[6] Badr E.A., Bedair M.A., Shaban S.M, Mater. Chem. Phys. 219 (2018) 444–460.
[7] M. Mobin, R. Aslam, J. Aslam, Mater. Chem. Phys. 223 (2019) 623–633.
[8] Yakun Zhu, Michael L. Free, Gaosong Yi, Corros. Sci. 102 (2016) 233–250.
[9] M. Mobin, Sheerin Masroor, Int. J. Electrochem. Sci. 7 (2012) 6920–6940.
[10] G. Gece, Corros. Sci. 50 (2008) 2981.
[11] M.K. Awad, R.M. Issa, F.M. Atlam, Mat. Corros. 60 (2009) 813.
[12] Awad M.K., Mustafa M.R., Abo Elnaga M.M., J. Mol. Struct. (THEOCHEM) 959 (2010) 66.
[13] M.S. Masoud, M.K. Awad, A.E. Ali, M.M.T. El-Tahawy, J. Mol. Struct. 1063 (2014) 51.
[14] M.A. Quraishi, R. Sardar, D. Jamal, Mater. Chem. Phys. 71 (2001) 309.
[15] R.M. Issa, M.K. Awad, F.M. Atlam, Mat. Corros. 61 (2010) 709.
[16] R.M. Issa, M.K. Awad, F.M. Atlam, Appl. Surf. Sci. 255 (2008) 2433.
[17] M.K. Awad, F.M. Mahgoub, M.M. El-iskandrani, J. Mol. Struct. (THEOCHEM) 531 (2000) 105.
[18] M.A. Hegazy, M. Abdallah, M.K. Awad, M. Rezk, Corros. Sci. 81 (2014) 54.
[19] Abass A. Olajire, J. Mol. Liq. 248 (2017) 775–808.
[20] M.J. Frisch, G.W. Trucks, H.B. Schlegel, G.E. Scuseria, M.A. Robb, J.R. Cheeseman, J.A. Montgomery Jr., T. Vreven, K.N. Kudin, J.C. Burant, J.M. Millam, S.S. Iyengar, J. Tomasi, V. Barone, B. Mennucci, M. Cossi, G. Scalmani, N. Rega, G.A. Petersson, H. Nakatsuji, M. Hada, M. Ehara, K. Toyota, R. Fukuda, J. Hasegawa, M. Ishida, T. Nakajima, Y. Honda, O. Kitao, H. Nakai, M. Klene, X. Li, J.E. Knox, H. P. Hratchian, J.B. Cross, C. Adamo, J. Jaramillo, R. Gomperts, R.E. Stratmann, O. Yazyev, A.J. Austin, R. Cammi, C. Pomelli, J.W. Ochterski, P.Y. Ayala, K. Morokuma, G.A. Voth, P. Salvador, J.J. Dannenberg, V.G. Zakrzewski, S. Dapprich, A.D. Daniels, M.C. Strain, O. Farkas, D.K. Malick, A.D. Rabuck, K. Raghavachari, J.B. Foresman, J.V. Ortiz, Q. Cui, A.G. Baboul, S. Clifford, J. Cioslowski, B.B. Stefanov, G. Liu, A. Liashenko, P. Piskorz, I. Komaromi, R.L. Martin, D.J. Fox, T. Keith, M.A. Al-Laham, C.Y. Peng, A. Nanayakkara, M. Challacombe, P.M.W. Gill, B. Johnson, W. Chen, M.W. Wong, C. Gonzalez, J.A. Pople, Gaussian 03, Revision B.01, Gaussian Inc, Pittsburgh, PA, 2003.
[21] A. Labena, M.A. Hegazy, H. Horn, E. Müller, J. Surf. Deterg. 17 (2014) 419–431.
[22] M.A. Hegazy, R.M. Sami, A. Labena, Mohammed A.M. Wadaan, Wael N. Hozzein, Mat. Sci. Eng. C 110 (2020) 110673.
[23] J.M. Luna, R.D. Rufino, L.A. Sarubbo, G.M.C. Takaki, Colloids Surf., B 102 (2013) 202–209.
[24] El-Tabei, A.S., Hegazy, M.A., Bedair, A.H., El Basiony, N., Sadeq, M.A. J. Mol. Liq. 331 (2021) 115692.
[25] M. El Faydy, M. Galai, A. El Assyry, A. Tazouti, R. Touir, B. Lakhrissi, M. Ebn Touhami, A. Zarrouk, J. Mol. Liq. 219 (2016) 396–404.
[26] Xu. Bin, Yan Ji, Xueqiong Zhang, Xiaodong Jin, Wenzhong Yang, Yizhong Chen, RSCAdv. 5 (2015) 56049.
[27] N.A. Odewunmi, S.A. Umoren, Z.M. Gasem, J. Environ. Chem. Eng. 3 (2015) 286–296.
[28] M.A. Hegazy, Ahmed Abdel Nazeer, K. Shalabi, J. Mol. Liq. 209 (2015) 419.
[29] M.A. Bedair, S.A. Soliman, M.A. Hegazy, I.B. Obot, A.S. Ahmed, J. Adhes, Sci. Tech. 33 (2019) 1139–1168.
[30] Hany M. Abd El-Lateef, Kamal A. Soliman, Ahmed H. Tantawy, J. Mol. Liq. 232 (2017) 478–498.
[31] M. Rbaa, F. Benhiba, I.B. Obot, H. Oudda, I. Warad, B. Lakhrissi, A. Zarrouk, J. Mol. Liq. 276 (2019) 120–133.
[32] A.S. El-Tabei, M.A. Hegazy, Chem. Eng. Commun. 7 (2015) 851.
[33] M.A. Hegazy, A.Y. El-Etre, M. El-Shafaie, K.M. Berry, J. Mol. Liq. 214 (2016) 347–356.
[34] M.A. Hegazy, A.S. El-Tabei, A.H. Bedair, M.A. Sadeq, Corros. Sci. 54 (2012) 219–230.
[35] M.R. Noor El-Din, A.M. Al-Sabagh, M.A. Hegazy, J. Disp. Sci. Tech. 33 (2012) 1444–1451.
[36] Samy S.M., Ismail Aiad, Mohamed M. El-Sukkary, E.A. Soliman, Moshira Y. El-Awady, J. Mol. Liq. 203 (2015) 20–28.
[37] O. Kaczerewska, R. Leiva-Garcia, R. Akid, B. Brycki, J. Mol. Liq. 247 (2017) 6–13.
[38] M.A. Hegazy, I. Aiad, J. Ind. Eng. Chem. 31 (2015) 91–99.
[39] M. Abdallah, M.A. Hegazy, M. Alfakeer, H. Ahmed, Green Chem. Lett. Rev. 11 (2018) 457–468.
[40] M.A. Hegazy, S.S. Abd El Rehim, A.M. Badawi, M.Y. Ahmed, RSC Adv. 5 (2015) 49070–49079.
[41] Z. Hu, Y. Meng, X. Ma, H. Zhu, J. Li, C. Li, D. Cao, Experimental and theoretical studies of benzothiazole derivatives as corrosion inhibitors for carbon steel in 1 M HCl, Corros. Sci. 112 (2016) 563–575.
[42] A.S. El-Tabei, M.A. Hegazy, A.H. Bedair, M.A. Sadeq, Egypt. J. Chem. 63 (2020) 3685–3701.
[43] Hegazy M.A., El-Etre A.Y., Berry K.M. J. Basic Environ. Sci. 2 (2015) 36–51.
[44] M.A. Hegazy, E.M.S. Azzam, N.G. Kandil, A.M. Badawi, R.M. Sami, J. Surfact. Deterg. 19 (2016) 861–871.
[45] Nashwa S. Bin-Hudayb, Entsar E. Badr, M.A. Hegazy, Materials 13 (2020) 2790–2817.
[46] M.A. Hegazy, S.S. Abd El-Rehim, Emad A. Badr, W.M. Kamel, Ahmed H. Youssif, J. Surfact. Deterg 18 (2015) 1033–1042.
[47] M.T. Majd, T. Shahrabi, B. Ramezanzadeh, Appl. Surf. Sci. 464 (2019) 516533.
[48] M.T. Majd, T. Shahrabi, B. Ramezanzadeh, J. Alloys. Compd. 783 (2019) 952968.
[49] V.S. Sastri, J.R. Perumareddi, Corrosion. 53 (1996) 671.
[50] A. Lalitha, S. Ramesh, S. Rajeswari, Electrochim. Acta 51 (2005) 47.
[51] D.Q. Zhang, L.W. Gao, G.D. Zhou, Corros. Sci. 46 (2004) 3031.
[52] G. Gao, C. Liang, Electrochim. Acta 52 (2007) 4554.
[53] G. Gece, S. Bilgiç, Corros. Sci. 51 (2009) 1876.
[54] A.S. El-Tabei, M.A. Hegazy, A.H. Bedair, N.M. El Basiony, M.A. Sadeq, J. Mol. Liq. 331 (2021) 115692.
[55] C. Morell, A. Grand, A.T. Labbe, J. Phys. Chem. A 109 (2005) 205.
[56] E.A. Badr, J. Indust. Eng. Chem. 20 (2014) 3361–3366.
[57] Hegazy M.A., Rashwan S.M., Meleek S., Kamel M.M., Mater. Chem. Phys. 267 (2021) 124697.
[58] A. Yıldirim, S. Ozturk, M. Cetin, J. Surfact. Deterg. 16 (2013) 13–23.